PPPL--3266

October 6, 1997

ITER L-Mode Confinement Database

S.M. Kaye and the ITER Confinement Database Working Group*

Abstract

This paper describes the content of an L-mode database that has been compiled with data from Alcator C-Mod, ASDEX, DIII, DIII-D, FTU, JET, JFT-2M, JT-60, PBX-M, PDX, T-10, TEXTOR, TFTR, and Tore-Supra. The database consists of a total of 2938 entries, 1881 of which are in the L-phase while 922 are ohmically heated only (OH). Each entry contains up to 95 descriptive parameters, including global and kinetic information, machine conditioning, and configuration. The paper presents a description of the database and the variables contained therein, and it also presents global and thermal scalings along with predictions for ITER. The L-mode thermal confinement time scaling, determined from a subset of 1312 entries for which the $\tau_{E,th}$ are provided, is

$$\tau_{E,th} = .023 I_p^{0.96} B_T^{0.03} R^{1.83} (R/a)^{0.06} \kappa^{0.64} \overline{n}_e^{0.40} M_{eff}^{0.20} P^{-0.73} \quad (1)$$

in units of sec, MA, T, m, -, -, $10^{19}\ m^{-3}$, AMU, MW.

* M. Greenwald and the Alcator C-Mod Group, Plasma Fusion Center, MIT, USA
U. Stroth, O. Kardaun, A. Kus and the ASDEX Group, Max-Planck Institut, Garching, Germany
D. Schissel, J. DeBoo and the DIII and DIII-D Groups, General Atomics, USA
G. Bracco and the FTU Group, EURATOM-ENEA, Frascati, Italy
K. Thomsen, J.G. Cordey and the JET Group, Abingdon, Oxon, UK
Y. Miura, T. Matsuda, H. Tamai and the JFT-2M Group, JAERI, Japan
T. Takizuka, T. Hirayama, M. Kikuchi, O. Naito and the JT-60 Group, JAERI, Japan
S. Kaye and the PBX-M, PDX, and TFTR Groups, PPPL, Princeton Univ., USA
A. Chudnovskii and the T-10 Group, Kurchatov Inst., Russia
J. Ongena and the TEXTOR Group, ERM/KMS - EURATOM, Belgian State, Belgium
G. Hoang and the Tore-Supra Group, EURATOM-CEA, St. Paul-lez-Durance, France

DISCLAIMER

DISCLAIMER

Portions of this document may be illegible in electronic image products. Images are produced from the best available original document.

Contents

1. Introduction

This report summarizes the activities over the past two years of the ITER Working Group on Confinement Databases and Modeling in assembling and analyzing an updated L-mode database in collaboration with the Alcator C-Mod, ASDEX, DIII, DIII-D, FTU, JET, JFT-2M, JT-60, PBX-M, PDX, T-10, TEXTOR, TFTR, and Tore-Supra groups.

Previous versions of the L-mode databases and analyses of confinement scaling relied exclusively on the global energy confinement time as determined by the plasma diamagnetism and/or MHD equilibrium calculations, which included contributions from both the thermal and fast (e.g., NBI) ion species [1–5]. In addition, the databases contained a relatively small number of global parameters describing the discharges; little detailed information was given concerning machine conditioning, wall materials, and other discharge information. The results of the analyses of these databases led to scaling expressions that, under the assumption of a power law form, were quite similar. As the underlying datasets were changed, so did the various regression coefficients to some extent, but all the scalings essentially showed the same qualitative and quantitative trends. The most recent and widely used L-mode scaling was developed by Yushmanov et al [3], known as ITER89-P, and given by

$$\tau_E^{ITER89-P} = 0.038 I_p^{0.85} R^{1.5} (R/a)^{-0.3} \kappa^{0.5} \overline{n}_e^{0.1} B_T^{0.2} M_{eff}^{0.5} P^{-0.5} \qquad (2)$$

in units of MA, m, m, -, 10^{19} m^{-3}, T, AMU, MW. The isotopic dependence was assumed, based on the results of Wagner et al. [6], and was fixed in the regression, as was the κ dependence.

Subsequent to these L-mode data compilation and analyses was a similar effort that was focussed on H-mode data. The original H-mode database, ITERHDB.1, [7] contained confinement data assembled from six tokamaks, and an updated version, ITERHDB.2, was released in 1994 [8]. The H-mode database assembly and analysis effort was significantly more detailed and sophisticated than those of the L-mode efforts. Because of all the hidden parameters, MHD instabilities, configurational effects, etc. that are specific to H-modes, much greater care was employed in selecting which discharges were to be included. Furthermore, a careful selection of standard subsets for analysis was undertaken (for ELMy and ELM-free discharges), which constrained discharges on the basis of time stationarity, fast ion content, fraction of radiated power, edge q, and proximity to the β-limit, to name a few. A detailed description of each data entry was included; each record contained up to 111 descriptive parameters including global and, where possible, local kinetic information, machine condition and

configuration. Thus, from this data, it was possible to develop scalings for the thermal as well as the global confinement times for the ELMy and the ELM-free standard data subsets.

The intent of this L-mode data compilation is to follow the lead of the H-mode effort in developing a database significantly more detailed than previous ones, and one from which both thermal and global scalings can be determined. The purpose of this paper is to present this database to the community along with a statistical description of the database and scaling results. In Section 2 of the paper we present descriptions of the devices from which the data were obtained, in Section 3 we present a description of the database, its data ranges and conditioning. In Section 4 we present the scaling results, and in Section 5 we present projections to ITER. In the appendix we present the detailed variable list for each entry; as will be seen, the variable list is similar to that for the H-mode database. Updates to the database will include more Ohmic and L-mode data from Alcator C-Mod, ASDEX-U, JET, JT-60U, START, TCV, TdeV, TEXTOR, TFTR and Tore-Supra.

2. Device Descriptions

Below are brief descriptions of the fourteen devices that have contributed data to the L-mode database. Appendix A gives the translation between the variables symbols used in the text and the database variable definitions given in Appendix B.

2.1. Alcator C-Mod

The Alcator C-Mod dataset consists of 190 time slices from 151 discharges taken during the 1993 and 1994 campaigns [9]. This includes data taken shortly after the device went into full operation in May 1993 and covers ohmic and preliminary ICRH heating phases. C-Mod ran during this period with an untreated Molybdenum first wall composed of approximately 7,000 tiles and covering all plasma "wetted" surfaces. The dataset contains a mix of limited, single and double null diverted discharges.

The data cover a fairly wide range in most global parameters with $0.36 \leq I_p\ (MA) \leq 1.0$, $3.4 \leq B_T\ (T) \leq 5.4$, $0.19 \leq a\ (m) \leq 0.24$, $0.65 \leq R\ (m) \leq 0.70$, $4 \leq \overline{n}_e\ (10^{19}\ m^{-3}) \leq 27$, $1.1 \leq \kappa \leq 1.7$, and $0 \leq P_{icrh}\ (MW) \leq 1.8$. No H-transitions were observed in the diverted discharges since $P_{icrh} < P_{threshold}$, where $P_{threshold}$ is the minimum power required for an L- to H-mode transition. Ohmic data is available in hydrogen and deuterium, but the ICRH heated discharges are all deuterium with hydrogen minority (1 to 5%).

Most discharges in this set are in steady state with respect to stored energy, density and poloidal field evolution. The data submitted are typically averaged over several energy confinement times. Data with $\overline{n}_e > 1 \times 10^{20}\ m^{-3}$ (most of the dataset) have $T_e \simeq T_i$. Stored energies are calculated from integration of kinetic profiles and from analysis of the magnetic equilibrium. The Fokker-Planck Program-RF (FPPRF) [10] analysis finds ion tail energies typically under 15% of the total stored energy, with much lower fraction seen at the higher densities. This data set is well fit by $\tau_E \sim I_p{}^1/P_{tot}^{.5}$, with negligible density or κ dependence.

2.2. ASDEX

The ASDEX contribution to the ITER L-mode database consists of 72 time slices from 26 different NBI heated discharges taken in 1989 and 1990. For each discharge, the data for the preceding ohmic phase are also given. The discharges are a representative subset for the L-mode confinement in the closed divertor configuration, DV-IIc. They are a subset from a large ASDEX L-mode database [11] and yield a scaling expression very similar to the one published [11]. Compared to the confinement in ASDEX with a more open divertor configuration, the confinement time of data from the closed divertor show a weaker current scaling, a weaker power degradation, and a 10 to 15% improved confinement [11]. It should be noted that the terms "open" and "closed" used here are relative, as there has been no quantification, through parameters such as compression ratio, of the divertor action across all divertor machines.

The selection criterion for the time slices was to fill uniformly the parametric space of the regression variables. Hence, the dataset is well conditioned with the strongest correlation of 57% between current and plasma ion mass. The other correlations are below 30%. Both $H \rightarrow H$ and $D \rightarrow D$ injection discharges are included. The parameter ranges are $0.32 \leq I_p\ (MA) \leq 0.46$, $0.26 \leq P_{nbi}\ (MW) \leq 2.7$, $1.7 \leq B_T\ (T) \leq 2.7$, and $1.3 \leq \overline{n}_e\ (10^{19}\ m^{-3}) \leq 9.1$, where P_{nbi} is the neutral beam power absorbed in the plasma (injected power less shine-through). The set of ASDEX L-mode discharges were obtained from experiments with reversed grad-B drift, where $P_{nbi} < P_{threshold}$.

Because of tangential injection, the diamagnetic energy content should be used in the regression. All data are calculated in the same way as for the H-mode database [7, 8].

2.3. *DIII*

The Doublet III contribution to the ITER L-mode database consists of 210 time slices taken from 210 discharges. There is one single-null discharge with the remainder resting on the outside single blade limiter. The discharges were taken from operating periods in 1982-1983 where a combination of TiC-coated graphite tiles and Inconel tiles were used as armor to protect the Inconel vacuum vessel. The TiC-coated graphite tiles were positioned at three toroidal locations. Titanium gettering was routinely used to condition the plasma facing components. The discharges were operated in the upper half of the doublet shaped vessel, and when the plasma elongation approached 1.8, the separatrix began to get close to the last closed flux surface.

The data cover wide ranges in global parameters with $0.2 \leq I_p\ (MA) \leq 0.8$, $0.3 \leq P_{nbi}\ (MW) \leq 4.5$, $0.6 \leq B_T\ (T) \leq 2.4$, $2.5 \leq \overline{n}_e\ (10^{19}\ m^{-3}) \leq 9.9$, and $1.0 \leq \kappa \leq 1.8$. All data have hydrogen neutral beams injected into deuterium plasmas.

Experimental results from Doublet III [12, 13] found that the plasma stored energy and confinement time increased with plasma current and were independent of density and magnetic field. The stored energy increased with power and for the limited range in power available the data was consistent with an offset linear and power law functional representation.

2.4. *DIII-D*

The DIII-D contribution to the ITER L-mode database consists of 161 time slices taken from 137 discharges. The discharges consist of single-null, double-null, and inside wall limited with the majority being in the single null configuration. The discharges were taken from operating periods in 1986-1987 and 1991-1993. During this time span different amounts of graphite tile vessel wall armor covered the top, inside, and bottom of the inconel vessel walls.

The data cover wide ranges in global parameters with $0.6 \leq I_p\ (MA) \leq 2.0$, $0.9 \leq P_{nbi}\ (MW) \leq 14.0$, $1.3 \leq B_T\ (T) \leq 2.2$, $1.5 \leq \overline{n}_e\ (10^{19}\ m^{-3}) \leq 6.2$, and $1.5 \leq \kappa \leq 2.1$. A variety of combinations of plasma mass and beam mass are included in the data with H→H, H→D, D→D, and He→He all being represented. The database includes values of q_{95} down to three. In general the data taken at specific time slices are not averaged in time, with the exception of MHD data determined from an equilibrium MHD code. Magnetic probe information required as input to the MHD code is averaged over $\pm$ 5 *msec.*

The ohmic power given in the database is determined from the plasma resistivity assuming the electric field is constant across the plasma. An estimate of the volume

averaged electron temperature is obtained from the MHD value of total stored energy assuming a dilution factor of one and Z_{eff} is determined from central chord visible bremsstrahlung measurements. Estimates of the fast ion energy content (WFFORM) and anisotropy (WFANI) are calculated in the same way as for the H-mode database (ITERHDB.2) [8].

Except for the very early operation, L-mode confinement [14] experiments were not routinely operated on DIII-D. For that reason the majority of the data collected for the L-mode database does not consist of dedicated parameter scans.

2.5. FTU

The FTU [15] contribution to the ITER L-mode database consists of 255 time slices from 227 discharges. All the data are in ohmic regime and have been selected from the results of the period 1993-1994, considering only stationary plasma conditions with sawtooth activity. Most of the data concern deuterium plasma but a set of hydrogen data, 22 time slices, is also provided [16].

FTU plasmas have an almost circular cross section, fixed by a system of metallic poloidal limiters (Inconel for 228 discharges and Molybdenum for the remaining 27). The wall material is stainless steel. A few discharges refer to the case when the siliconization of the whole chamber has been performed. The global confinement appears to depend weakly on the different wall and limiter conditions. The radiated fraction of the total input power is in the range 30 to 85%, and very strong MARFE conditions have been discarded. The data cover wide ranges in global parameters $0.26 \leq I_p\ (MA) \leq 1.2,\ 2.5 \leq B_T\ (T) \leq 7.1,\ 2.3 \leq \overline{n}_e\ (10^{19}\ m^{-3}) \leq 23$, and $2.5 \leq q_{95} \leq 6.2$.

Kinetic measurements have been used to estimate the plasma energy content. Electron temperature profiles are obtained from ECE for $B_T \geq 4\ T$ while at lower field, Thomson Scattering data are used. When both measurements are available, they are in good agreement (5% at $B_T = 6\ T$). The electron density is measured by a 5 channel DCN interferometer. Z_{eff} is obtained assuming Spitzer resistivity, since the Bremsstrahlung value has been measured only in a limited subset of discharges and it is in good agreement with Spitzer resistivity. Plasma dilution has been estimated from Z_{eff} assuming a single dominant impurity, usually Ni. Ion temperature profiles are obtained by solving the ion power balance equation assuming neoclassical ion thermal diffusivity (Chang-Hinton with corrections due to impurities). The computed neutron flux is generally in agreement with the experiment. The sawtooth inversion radius is obtained from a 12 channel ECE polychromator. WMHD is obtained from the

equilibrium reconstruction code, which is able to separate β_{pol} and $l_i/2$ if $\kappa \geq 1.05$, as is the case for most of the discharges. All the time dependent data have been averaged over a 0.1 s interval. Most of FTU operation has been performed at $B_T = 6\ T$, so that the largest contribution to the database is at this field value, providing a wide scan of I_p values. Data at other fields provide a B_T scan at fixed q_{95}. The linear dependence of confinement time on plasma density can be observed at all current and field values, while the saturated ohmic regime is observed only at $B_T \geq 4\ T$.

2.6. *JET*

The JET contribution to the ITER L-mode database consists of 433 time slices from 108 discharges taken during the 1986 experimental campaign [17, 18]. In 1986, the vessel inner wall on the high field side was covered with carbon tiles. Eight evenly toroidally spaced localized carbon limiters together with the carbon frames of three ICRH antennae formed the outboard or low field side wall protection. Before the experiments with x-point configurations took place, carbon tiles were also installed at the top and bottom. All the data from the 108 discharges have been taken from the limiter phase, where the plasma was limited on the outboard. For each discharge, data from one ohmic reference point just prior to auxiliary heating, and up to three points at each subsequent auxiliary heating power level have been provided. Most data have been smoothed over $\pm$ 100 msec. Notice that a few points with negligible ICRH power have been labelled with PHASE=OH. The ohmic power has been corrected for inductance effects. During NBI heating the ohmic power given in the database is very uncertain. All the discharges had deuterium as the main gas. The L-mode data cover the following ranges in global parameters: $1 \leq I_p\ (MA) \leq 5$, $1.7 \leq B_T\ (T) \leq 3.5$, $1.7 \leq \overline{n}_e\ (10^{19}\ m^{-3}) \leq 5.1$, and $2.5 \leq q_{95} \leq 8$. The L-mode data were obtained with either NBI, ICRH or combined NBI and ICRH. The NBI heated data is either with hydrogen or deuterium beams ($0.9 \leq P_{nbi}\ (MW) \leq 8.3$), whereas the ICRH data were obtained using either a hydrogen minority ($0.001 \leq P_{icrh}\ (MW) \leq 5.3$) or a helium-3 minority ($0.002 \leq P_{icrh}\ (MW) \leq 5.1$) heating scheme. Notice that the minority gas heated by the ICRH was introduced to the discharge by gas puffing. Although it has been impossible to establish exactly how much each discharge contained, it was typically 5 to 10%. Two of the three antennae could be run in dipole or quadrapole configuration, and the third in either monopole or dipole. This information is not included in the database but can be provided on request. In the normal mode of operation of JET in 1986, the plasma current was negative and the toroidal magnetic field positive. The contributed data include NBI heated data with

positive plasma current and negative toroidal magnetic field. Hence for this data the NBI was counter injected. Finally estimates of the fast ion energy content have been calculated in the same way as for the H-mode confinement database [7, 8].

2.7. JFT-2M

There are two kinds of contribution from the JFT-2M tokamak to the ITER L-mode database. One comes from the set of data contributed to the ITER threshold database [19] for which PHASE="L". The total contribution from this dataset is 102 observations with $\kappa < 1.5$, $\delta < 0.73$, $0.11 \leq P_{nbi}\ (MW) \leq 0.3$, $0.12 \leq I_p\ (MA) \leq 0.3$, $0.66 \leq B_T\ (T) \leq 1.41$, and $\overline{n}_e\ (10^{19}\ m^{-3}) \leq 4.3$. The plasma configuration is a divertor configuration, primarily single null but with a few double null discharges. Since the L/H power threshold is not high in a divertor configuration, the power range of the L-mode data is very limited. The data with high heating power are from hydrogen plasmas with unfavorable B_T direction, or with small gaps (small distance between plasma and limiter), or with no gettering.

The other dataset contributed is from a threshold study in a limiter configuration to assess the effect of elongation [20]. The total contribution is 36 observations at a limiter configuration with $\kappa < 1.44$, $\delta < 0.54$, $0.25 \leq P_{nbi}\ (MW) \leq 1.0$, $0.23 \leq I_p\ (MA) \leq 0.36$, $0.96 \leq B_T\ (T) \leq 1.34$, and $\overline{n}_e\ (10^{19}\ m^{-3}) \leq 4.5$. Since the measurement of a confined plasma energy is based on a equilibrium calculation, WDIA, WMHD, TAUDIA and TAUMHD are set to missing when $\kappa < 1.2$ since the separation of β_{pol} and l_i is highly uncertain for data with low elongation.

2.8. JT-60

A portion of the JT-60 contribution was the circular cross-section data that went into the development of the ITER89P scaling [3]. During the ITER CDA, additional data in an elongated elongated configuration (so-called "Lower X-point configuration") were submitted to the ITER L-mode Database. Thermal energy confinement data of L-mode and ohmic plasmas, both with circular and with elongated cross sections, were added to the database after the ITER EDA started. A detailed description of those data for circular plasmas is found in Kikuchi et al [21].

From SHOT 1050 to 5886 in the database, cross sections were circular ($\kappa = 1$) with LIM (limiter) and SNO (Outer-Single Null) CONFIGURATIONs. From SHOT 6861 to 11209, the cross sections were elongated ($\kappa = 1.29$ to 1.45) with SN (Lower-Single Null) configurations. The plasma volume for former plasmas was rather large

(34 to 50 m^3), while that for latter was rather small (24 to 34 m^3). Initially the wall material (WALMAT=LIMMAT=DIVMAT) was TiC/Mo (Molybdenum coated with Titanium-Carbide) from SHOT 1050 to 3995. This was replaced by C (Carbon) from SHOT 4565 to 11209. There was no gettering (EVAP=NONE) in these discharges.

A major characteristic of the JT-60 data is the wide range of parameters, except for gas species (all were Hydrogen): $2.86 < R\ (m) < 3.16$, $0.53 < a\ (m) < 0.91$, $3.3 < (R/a) < 5.8$, $1 < \kappa < 1.45$, $2.3 < B_T\ (T) < 4.7$, $0.66 < I_p\ (MA) < 3.1$, $0.5 < \overline{n}_e\ (10^{19}\ m^{-3}) < 9.0$, $0.56 < P_L\ (MW) < 26.6$, and $0.11 < W_{tot}\ (MJ) < 2.6$, where P_L is the total heating power corrected for dW/dt but not for charge-exchange, bad orbit losses or radiated power. Operation in hydrogen and non-optimized wall conditions caused the L-H threshold power to be greater than the heating power for this set of JT-60 discharges. Based on the above JT-60 data, a scaling of thermal energy confinement was obtained, which fits well L-mode data as well as ohmic data of JT-60 [22].

2.9. PBX-M

The PBX-M dataset consists of 31 time slices from 31 discharges taken during the run period in 1988-1989 in a double-null, open divertor configuration [23]. All discharges had deuterium neutral beams injected into a deuterium plasma, with variable mixtures of perpendicular ($R_{tangency} = 0.348\ m$) and tangential ($R_{tangency} = 1.30\ m$) beams into plasmas with $R_0 = 1.65\ m$ and $a = 0.28\ m$. PBX-M is a high aspect ratio device, with $R/a \simeq 5.5$. The L-mode discharges covered a narrow range of operating space, with $0.32 \leq I_p\ (MA) \leq 0.38$, $1.25 \leq B_T\ (T) \leq 1.37$, $2.87 \leq \overline{n}_e\ (10^{19}\ m^{-3}) \leq 7.50$, $1.12 \leq P_{nbi} + P_{oh}\ (MW) \leq 4.01$, and $3.67 \leq q_{95} \leq 5.55$. The PBX-M plasmas were slightly indented, typically 16 to 19%, on the outer flux surface, but the indentation was greater than zero only on the outer several flux surfaces. The elongation of these plasmas was ~ 1.6. In general, no significant correlations are found among the primary engineering variables.

The discharges were essentially in steady-state in terms of the global energy and density. Thermal confinement times are based on equilibrium magnetics calculations of total energy, and estimates of fast ion energy content and bad orbit and charge-exchange loss based on TRANSP runs. The thermal confinement times show a strong dependence on $P_{L,th}\ (P_{nbi} + P_{oh} - P_{bo} - P_{cx} - dW/dt)$ and $\overline{n}_e$, with $\tau_{E,th} \sim \overline{n}_e^{0.35} P_{L,th}^{-0.84}$.

2.10. PDX

The PDX dataset consists of 51 time slices from 51 discharges, covering OH (11 time slices) and auxiliary heated (40 time slices) plasmas. The L-mode experiments in PDX were performed during 1981-1982 in a limited, circular cross-section configuration. During the high field (2.2 T), high power (≤ 6 MW) experiments performed in 1981, the discharges were run with uncooled top and bottom graphite rail limiters, while during the high-β_t experiments carried out in 1982, only the top limiter with water cooling was used. Titanium gettering was typically employed. A more comprehensive description of the PDX tokamak is given in Meade et al. [24] and Kaye et al. [25]. In PDX, all four beams were injected in a near-perpendicular direction, with a tangency radius of 0.348 m, giving an angle of 14° from perpendicular at the center of the vessel. All discharges had hydrogen as the working gas, and deuterium was injected by the neutral beams.

One of the goals of these PDX experiments was to ascertain the parametric dependence of the energy confinement time; as such, the experiments were carried out in a systematic fashion that covered a relatively wide range in parameter space. The operating parameter ranges for these experiments were $R_0 = 1.4$ m, $a = 0.4$ m, $0.23 \leq I_p$ $(MA) \leq 0.50$, $0.71 \leq B_T$ $(T) \leq 2.2$, $2.3 \leq \overline{n}_e$ $(10^{19}$ $m^{-3}) \leq 5.6$, $1.22 \leq P_{nbi} + P_{oh}$ $(MW) \leq 5.69$, and $1.9 \leq q_{95} \leq 4.2$. Little correlation was found among the primary engineering variables, although the $B_T = 2.2$ T discharges were run at lower density (~ 2 *to* 3×10^{19} m^{-3}) than were the lower field discharges (~ 3.5 *to* 5.5×10^{19} m^{-3}).

Confinement times (thermal and total) were calculated using the TRANSP analysis code for each discharge. Calculations of beam stored energy and fast ion bad orbit and charge-exchange losses were done also in each TRANSP run. The TRANSP analysis was based on input T_e and n_e profiles, a Z_{eff} that was measured by visible bremsstrahlung but assumed to be flat, and a central ion temperature value. The T_i profile was not measured at that time, but rather was computed using a value of the neoclassical [26] multiplier that was obtained by matching the central ion temperature value. The multiplier was assumed to be constant across the profile, and was typically 1 to 3. The calculated perpendicular stored energy was within a factor of 10% of the value obtained from the diamagnetic loop measurement. The thermal energy confinement time showed a strong, nearly linear, dependence on plasma current, a weak dependence on plasma density and toroidal field, and a $P_{L,th}^{-(0.5-0.6)}$ dependence. The PDX thermal confinement times generally increase (relative to the thermal confinement scaling that will be presented later on) with increasing $T_i(0)/T_e(0)$.

2.11. T-10

The T-10 contribution [27] consists of 40 time slices from 20 discharges. For each shot, two time slices are provided: one ohmic and one ECRH-heated L-mode. Both points achieve nearly steady-state conditions. The experimental values of the time derivatives of the line-averaged density and stored energy are small. The stored energy derived from the diamagnetic measurement and from kinetic measurements were nearly the same, and, therefore, WDIA was set to be equal to WKIN to emphasize the absence of fast particles. Calculations were performed to verify this assumption.

The data contained in the database were obtained from a power scan performed in May 1988. $P_{rad} \leq 0.4\ MW$ for all but one shot; for shot 47405, with $a = 0.22$, $P_{rad} \simeq 0.9\ MW$. The parameter ranges are: $0.15 \leq I_p\ (MA) \leq 0.43$, $2.76 \leq B_T\ (T) \leq 3.07$, $1.47 \leq \overline{n}_e\ (10^{19}\ m^{-3}) \leq 5.59$, $0.58 \leq P_{ecrh}\ (MW) \leq 1.89$, and $2.14 \leq q_{edge} \leq 6.34$.

2.12. TEXTOR

The TEXTOR dataset consists of 260 time slices taken from 165 different discharges. The data are from L-mode discharges with either ICRH or neutral beam heating, and neutral beam plus ICRH (low field side launch) I-mode discharges [28]. The main working gas in these discharges was deuterium with a small percentage of hydrogen ($< 5\%$).

Whenever possible, two data points for each shot were provided : one during the ohmic phase of the shot and one during the auxiliary heated phase. Both points were taken during the stationary part of each phase. There are 85 ohmic data points, 82 data points from L-mode discharge phases, and 93 from I-mode discharge phases. Samples are averaged over intervals of 100 msecs.

The plasma energy content from MHD is within the error bars equal to the diamagnetic energy, indicating that the plasma particle distribution does not contain significant high energy tails. Both measurements represent thus a measurement of the thermal energy content. Therefore, WTH=WTOT=WDIA. Due to the absence of large energetic tails, the neutron yield is a thermal neutron yield, and this enabled us to deduce a central ion temperature. The values for Z_{eff} are calculated from resistivity and cross-checked with soft x-ray data.

The ranges of the most important plasma parameters are as follows :

$0.2 \leq I_p\ (MA) \leq 0.5$, $1.9 \leq B_T\ (T) \leq 2.36$, $0.25 \leq P_{icrh}\ (MW) \leq 2.1$, $1.65 \leq P_{nbi}\ (MW) \leq 3.3$, $0.5 \leq \overline{n}_{ohm}\ (10^{19}\ m^{-3}) \leq 4.5$, $1.6 \leq \overline{n}_{Lmode}\ (10^{19}\ m^{-3}) \leq 5.9$, $1.45 \leq \overline{n}_{Imode}\ (10^{19}\ m^{-3}) \leq 4.62$, and $2.7 \leq q_{cyl} \leq 6.6$.

2.13. *TFTR*

The TFTR dataset consists of 189 time slices from 168 discharges taken during the run period from 1989 to 1992, all in a limited, circular cross-section configuration and covering a wide range of experiments. The L-mode experiments in TFTR were carried our using a carbon toroidal belt limiter on the inner wall, and for the earlier set of experiments, two carbon poloidal rail ring limiters on the outer wall. Machine conditioning during this period was performed using helium glow discharge cleaning. The neutral beams used for these experiments varied in tangency radius, but were always injected in the co-direction. Typically, the beam ion distribution was calculated to be isotropic. In all experiments, deuterium was injected by the neutral beams. Strong gas puffing was employed in order to establish a high recycling regime ($R \sim 1$) and L-mode operation.

The collection of TFTR experiments consisted of current, density, and power scaling experiments [29], size and aspect ratio experiments [30], non-dimensional transport scaling experiments [31, 32], and isotope scaling experiments [33]. The working gas in all but the isotope scaling experiments was deuterium. In the isotope scaling experiment, deuterium and hydrogen working gasses were used. Hydrogen plasmas were run by strong gas puffing of hydrogen after several hours of glow discharge cleaning. No tritium working gas discharges are included in this release of the database.

The systematic L-mode experiments in TFTR covered a wide range of operating space, with $2.09 \leq R\ (m) \leq 3.18$, $0.41 \leq a\ (m) \leq 0.93$, $2.77 \leq (R/a) \leq 7.78$, $0.40 \leq I_p\ (MA) \leq 2.09$, $3.57 \leq B_T\ (T) \leq 4.82$, $1.47 \leq \overline{n}_e\ (10^{19}\ m^{-3}) \leq 8.97$, $2.16 \leq P_{nbi} + P_{oh}\ (MW) \leq 21.96$, and $2.35 \leq q_{95} \leq 10.16$. The plasma elongation in these experiments was ~ 1. No strong correlations among the primary engineering variables were found, although the highest power discharges tended to be at higher density and plasma current, and the highest aspect ratio (smallest) plasmas were run with lower currents.

The stored energy and confinement times in TFTR plasmas were calculated from both diamagnetic measurements and from profile measurements by the 1-D SNAP transport code [34]. Inputs to SNAP include T_e, n_e, T_i, v_ϕ, and P_{rad} profiles, Z_{eff} as measured by visible bremsstrahlung and assumed to be flat across the plasma, and other global discharge parameters. SNAP computes the beam ion energy by solving the Fokker-Planck equation, and also estimates the bad orbit loss of these ions. The thermal confinement times in this dataset show strong dependences on heating power, plasma current, and major radius, with weak dependences on the other variables,

scaling roughly as $\tau_{E,th} \sim I_p^{1.2} R^{1.2} M_{eff}^{0.2} \overline{n}_e^{0.15} P^{-0.7}$.

2.14. *Tore-Supra*

Tore-Supra [35] provides a combination of super conducting toroidal field coils and multi-megawatt radio frequency systems. The Lower Hybrid Current Drive, LHCD, system is 3.7 GHz, with $n_{\parallel} \simeq 1.8$. The Ion Cyclotron Resonant Frequency system is 35 to 80 MHz, operated in either the minority heating or Fast Wave Electron Heating (FWEH) mode. The dataset consists of 261 time slices taken during the stationary phase of 123 L-mode discharges, and of 24 improved confinement discharges obtained by current profile modification. The data are from discharges with an ohmic phase followed by an RF heating phase mainly consisting of LHCD. There are 92 ohmic points, 127 L-mode points, and 42 improved confinement data points (23 LHEP and 19 EP). Most of experiment have been performed with either helium or deuterium, with a small concentration of hydrogen ($\leq 5\%$).

The electron density profile is measured by far-infrared interferometers ($\lambda = 195\ mm$ with five vertical chords), and a twelve channel Thomsen scattering system with a spatial resolution of 6 cm. The electron temperature is measured by Thomson scattering and electron cyclotron emission (ECE) diagnostics. The ion temperature profile is deduced from six passive fast particle charge-exchange analyzers; it is available, however, for only low density deuterium/hydrogen plasmas. Line-averaged effective charge (Z_{eff}) is determined from the visible bremsstrahlung emission.

The total energy, deduced from magnetic and diamagnetic measurements, is close to the thermal energy since the contribution of fast particles is less than 10% for ICRH minority heating or LHCD. There are no fast particles during the FWEH experiments. Noting the electron heating is dominant during the RF phase (ions are weakly heated by equipartition), the thermal electron energy content is up to 75% of the total stored energy, and is well described by the global Rebut-Lallia-Watkins scaling [35]. The thermal confinement time is found to depend strongly on the plasma density, scaling as $\tau_E = 0.0227 R^{1.84} I_p^{1.2} B_T^{0.2} \overline{n}_e^{0.43} P^{-0.75}$. There is no elongation dependence since the Tore-Supra plasmas are circular.

The ranges of main plasma parameters are as follows: $0.32 \leq I_p\ (MA) \leq 1.7$, $2 \leq B_T\ (T) \leq 3.95$, $0.4 \leq P_{tot}\ (MW) \leq 9.8$, $1.5 \leq \overline{n}_e\ (10^{19}\ m^{-3}) \leq 4.9$, and $3 \leq q_{edge} \leq 9.9$.

DEVICE	TOTAL	OH	L	Improved L-mode
Alcator C-Mod	190	135	55	
ASDEX	98	26	72	
D-III	210	0	210	
DIII-D	161	0	161	
FTU	255	255	0	
JET	433	108	325	
JFT-2M	137	0	137	
JT-60	622	190	432	
PBX-M	31	0	31	
PDX	51	11	40	
T-10	40	20	20	
TEXTOR	260	85	82	93
TFTR	189	0	189	
Tore-Supra	261	92	127	42
TOTALS	2938	922	1881	135

Table 1: Breakdown of Entries by Device and PHASE

3. Database Description

3.1. Summary Statistics

The L-mode database consists of 2938 entries, 922 of which are OH heating only, and the remaining 2016 having auxiliary heating. Of the auxiliary heated entries, 1881 are in the L-phase, with the remaining being either EP (Enhanced Performance - 19 entries) or LHEP (Lower Hybrid Enhanced Performance - 23 entries) from Tore-Supra, or "I-Mode" from TEXTOR (93 entries). The number of entries for OH and L-phase for each device is given in Table 1. Although a description of the OH portion of the database and OH confinement scalings will be presented in later sections, a more comprehensive OH analysis will be performed once additional OH data from ASDEX-U, JET, JT-60U, START, TEXTOR, and Tore-Supra are assembled into the database update.

As can be seen in Table 1, the L-mode phase observations are dominated by JET and JT-60 in terms of number of entries; these two devices account for approximately 40% of the total L-mode entries. Relatively few L-mode discharges were contributed by Alcator C-Mod, PBX-M, PDX, and T-10. In Table 2 are shown the total number of entries by machine (first and second columns), and the number of entries eliminated

for that machine by applying subsequent constraints. For instance, for Alcator C-Mod, 135 entries are eliminated when the constraint L-only (i.e., no OH or improved L-mode discharges) is applied. In addition, the data is constrained for hydrogenic plasmas only (no He); for DIII-D, 14 entries are eliminated when this constraint is applied. A total of 75 entries, mostly from Tore-Supra, are eliminated also by this constraint. For the scaling analysis of $\tau_{E,th}$, an estimate of the thermal confinement time is required. This constraint eliminates 494 discharges, mostly from DIII and JT-60. The number of entries available for the analysis of the $\tau_{E,th}$ scaling is 1312. The subset is dominated by JET, with 325 discharges. As FTU is the only OH only device in the present database, and DIII could not provide $\tau_{E,th}$ data due to lack of estimates of fast ion energy, these devices have zero entries for determining the $\tau_{E,th}$ scaling. Note that there are discharges with additional heating that are not in the L-phase; 93 of them are I-mode discharges from TEXTOR. The rest, from Alcator C-Mod and JET, have very small amounts of RF power injected such that $P_{rf} << P_{oh}$. These discharges are classified as $PHASE = OH$. It is also worth noting that the percentage of observations from the biggest machines (JET, JT-60, TFTR, Tore-Supra) is approximately the same (57%) for both the total number of L-mode observations and in the subset which is going to be used for the $\tau_{E,th}$ analysis. Additionally, JET and JT-60 constitute approximately 40% in both distributions. Despite their constituting 40% of the standard subset, omitting either JET or JT-60 data has little effect on the parametric dependences of the thermal confinement time scaling. Omitting both datasets simultaneously has only a slightly larger effect, with the most noticeable one being a mere (10%) reduction in the size (R) scaling coefficient.

The subset described above contains both ion and electron preferential heating. The electron preferential heating discharges consist of entries of LH, ECRH, and ICRH heating from Alcator C-Mod, JET, T-10, TEXTOR, and Tore-Supra. There are not enough electron preferential heating discharges to perform a separate analysis, although results with and without these discharges included will be discussed in a later section.

For the subset of hydrogenic L-mode data for which $\tau_{E,th}$ is available (to be called the standard subset), 861 of the 1312 entries are limiter discharges, while 451 of them are diverted. This breakdown, by machine, is given in Table 3. In general, the diverted subset of data tends to come from machines of more modest size (except for those from JT-60) than the subset of limiter entries. Additionally, except for ASDEX and the 15 ergodic divertor discharges from Tore-Supra, the divertor subset of data consists of more elongated discharges. The effect of configuration on the confinement

DEVICE	TOTAL	L-only	no He	$\tau_{E,th}$ AVAILABLE	NET
Alcator C-Mod	190	135	0	0	55
ASDEX	98	26	0	0	72
D-III	210	0	0	210	0
DIII-D	161	0	14	18	129
FTU	255	255	0	0	0
JET	433	108	0	0	325
JFT-2M	137	0	2	8	127
JT-60	622	190	0	258	174
PBX-M	31	0	0	0	31
PDX	51	11	0	0	40
T-10	40	20	0	0	20
TEXTOR	260	178	0	0	82
TFTR	189	0	0	0	189
Tore-Supra	261	134	59	0	68
TOTALS	2938	1057	75	494	1312

Table 2: Number of Entries Eliminated by Data Constraints

scalings will be discussed in a later section.

The final breakdown, that by type of auxiliary heating, for the standard subset is given in Table 4. Neutral beam heating is the dominant auxiliary heating technique, with 1019 entries, or 78% of the subset using this method. ICRH (Ion Cyclotron) heating accounts for 12% of the total (160 entries), with the remaining 10% split between LH (Lower Hybrid), ECRH (Electron Cyclotron), and combined heating methods, NBIC and LHIC. Alcator C-Mod, T-10, TEXTOR, and Tore-Supra do not have any neutral beam heating.

3.2. Parameter Ranges

3.2.1. OH Plasmas

The ohmic section of database consists of 922 observations from the Alcator C-Mod, ASDEX, FTU, JET, JT-60, PDX, T-10, TEXTOR, and Tore-Supra while no ohmic data have been provided by DIII, DIII-D, PBX-M, TFTR and JFT-2M. The size of the ohmic section corresponds to about 1/3 of the entire database but its content is not a complete description of the typical ohmic energy confinement. In fact for some of the tokamaks the ohmic data have been provided mainly as a description

DEVICE	Limiter	Divertor
Alcator C-Mod	47	8
ASDEX	0	72
DIII-D	18	111
JET	325	0
JFT-2M	27	100
JT-60	60	114
PBX-M	0	31
PDX	40	0
T-10	20	0
TEXTOR	82	0
TFTR	189	0
Tore-Supra	53	15
TOTALS	861	451

Table 3: Breakdown of Standard Subset Entries by Device and CONFIG

DEVICE	Type of Heating
Alcator C-Mod	ICRH:55
ASDEX	NB:72
DIII-D	NB:129
JET	NB:257 ICRH:16 NBIC:52
JFT-2M	NB:127
JT-60	NB:174
PBX-M	NB:31
PDX	NB:40
T-10	ECRH:20
TEXTOR	ICRH:82
TFTR	NB:189
Tore-Supra	ICRH:7 LH:51 LHIC:10
TOTALS	NB:1019 ICRH:160 LH:51 ECRH:20 NBIC:52 LHIC:10

Table 4: Breakdown of Standard Subset Entries by Device and AUXHEAT

DEVICE	$B_T\ (T)$	$\overline{n}_e\ (10^{19}\ m^{-3})$	$I_p\ (MA)$	q_{edge}	$(\overline{n}_e q_{edge})_{SAT}$
Alcator C-Mod	3.5-5.5	4-27	0.35-1	4-10	40
ASDEX	1.6-2.2	1-6	0.3-0.45	2-3.4	10
FTU	2.5-7	2-27	0.27-1.2	2.7-6	40
JET	1.7-3.5	1-4	1-5	2-3.4	6
T-10	3	1.5-4	0.15-0.45	2.4-7	12
TEXTOR	2	1-5	0.2-0.5	2.7-6.5	12
Tore-Supra	4	2-3	1.6	3.8	8

Table 5: Deuterium Ohmic Data (627 entries)

DEVICE	$B_T\ (T)$	$\overline{n}_e\ (10^{19}\ m^{-3})$	$I_p\ (MA)$	q_{edge}	$(\overline{n}_e\ q_{edge})_{SAT}$
Alcator C-Mod	5	5-1.1	0.35-0.6	4.7-10	40
ASDEX	2.2	2.5-3.5	0.4	2.8	10
FTU	6	4-20	0.7	4.3	40
JT-60	3.8-4.7	0.4-0.8	0.85-2.3	3-7	7
PDX	0.6-2.2	1.5-3.5	0.2-0.5	2-4	8
Tore-Supra	4	3-4	1.6	3.8	7

Table 6: Hydrogen Ohmic Data (265 entries)

of the target plasma preceding the additional heated phase when the L-mode data have been obtained. Nevertheless it is worthwhile to analyse the content of this ohmic section, which can be considered to be a by-product of the main effort of collecting the L-mode database, and which contains validated data from a wide range of plasma parameters from several tokamaks.

Tables 5 and 6 show the ranges of the main plasma parameters for the data of deuterium and hydrogen plasma respectively. Some helium data from Tore-Supra are also available. The standard behaviour of the energy confinement in ohmic regime is characterized by a linear increase of τ_E with increasing density (LOC: linear ohmic confinement regime) followed by a saturation (SOC: saturated ohmic confinement regime). Most of the data in the database refers to the SOC regime with the exception of PDX, TEXTOR and T-10, which are mainly in LOC regime, and FTU and JT-60 that covers both regimes. For this reason it is not possible to use the database for a quantitative analysis of the parametrical dependence of the saturation density or a detailed analysis of the LOC regime. On the contrary, only a study of the SOC regime can be attempted.

Variable	Units	Number	Range	Mean	Standard Deviation
R_0	m	1312	0.67-3.18	2.24	0.72
a	m	1312	0.21-1.22	0.74	0.33
R/a		1312	2.41-7.78	3.33	0.86
κ		1312	0.95-2.08	1.27	0.28
I_p	MA	1312	0.12-5.01	1.43	1.04
B_T	T	1312	0.66-5.27	2.90	1.14
q_{95}		1230	1.89-10.16	4.33	1.33
$\overline{n}_e$	$10^{19}\ m^{-3}$	1312	1.0-18.52	3.96	2.19
M_{eff}	AMU	1312	1.0-2.0	1.67	0.39
P_{oh}	MW	1312	-0.06-4.31	0.79	0.68
P_{tot}	MW	1312	0.31-21.96	5.75	4.70

Table 7: Parameter Ranges for the Standard Subset

3.2.2. L-mode Plasmas

The parameter ranges for the standard subset, as defined in Section 3.1, along with their means and standard deviations, are given in Table 7. q_{95} was not provided in the TEXTOR dataset.

3.3. Data Collinearity

As discussed in Section 3 of the article describing the global H-mode database [7], two useful yardsticks for giving insight into the collinearity of what are believed to be the most important parameters in determining the global confinement scaling are the correlation and principal component matrices.

3.3.1. OH Plasmas

The subset containing only SOC data has been obtained by taking into account only data with $\overline{n}_e\ q_{edge} \geq (\overline{n}_e\ q_{edge})_{SAT}$ where the value of $(\overline{n}_e\ q_{edge})_{SAT}$ is given in Tables 5 and 6 for each tokamak. In Table 8 the correlation coefficients for the main plasma parameters are shown. The correlations are computed using the natural logarithms of the variables, since that is what will be used to determine the confinement scaling. Only half the matrix is shown because of its symmetry. Pairwise correlations with correlation coefficients > 0.7 are shown in bold. The main correlations are the coupling of $\overline{n}_e$ and I_p to the tokamak size and magnetic field, due to the characteristics of the typical tokamak operation space as described by the Hugill diagram.

Variable	$ln(RGEO)$	$ln(R/a)$	$ln(IP)$	$ln(BT)$	$ln(MEFF)$	$ln(NEL)$	$ln(KAPPA)$
$ln(RGEO)$	1.00						
$ln(R/a)$	-0.18	1.00					
$ln(IP)$	**0.74**	-0.64	1.00				
$ln(BT)$	-0.60	0.28	-0.35	1.00			
$ln(MEFF)$	-0.43	-0.40	-0.06	0.07	1.00		
$ln(NEL)$	**-0.89**	0.23	-0.58	0.69	0.41	1.00	
$ln(KAPPA)$	-0.30	-0.69	-0.19	-0.12	0.47	0.16	1.00

Table 8: Ohmic Data Correlation Matrix

3.3.2. L-mode Plasmas

In Table 9 is presented the correlation matrix for the standard L-mode subset. As can be seen, there is a general correlation between plasma current/magnetic field, device geometry, and heating power. Larger machines operate at higher currents, fields, and heating power, as expected. The highest plasma currents are found in devices at the lowest aspect ratio. These correlations necessarily introduce coupling among the exponents in these variables. The coupling, or correlation, of the independent variables is taken into account properly in the determination of the standard errors of the scaling coefficients for log-linear regression as long as the database is not severely ill-conditioned, and in this case it is not.

Principal component, or eigenvalue/eigenvector, analysis transforms the data into a set of orthogonal directions defined by various combinations of the independent variables. A discussion of this is found in the first ITER H-mode database paper [7]. Table 10 shows the results of the principal component (p.c.) analysis of the covariance matrix, where the p.c.s go from the largest (pc1) to the smallest (pc8), the smallest p.c.s corresponding to those directions of least variation. The second through ninth columns of the tables correspond to the eigenvector (i.e., pc1=0.20ln(RGEO) -0.12ln(R/a)+...). STD is the standard deviation of that p.c., and this corresponds to the magnitude of the variation in that direction. ERR is the ratio of λ_e to STD, where λ_e is the standard deviation of the measurement error in the p.c. direction. As discussed in the H-mode database article [7], collinearity problems exist if $ERR \geq 1$; as a rule, $ERR \leq 0.25$ indicates a well conditioned database. To compute ERR, it is assumed that the standard deviations of the measurement errors in R, R/a, I_p, B_T, M_{eff}, $\overline{n}_e$, κ, and $P_{L,th}$ are 0.5%, 1%, 1%, 1%, 10%, 5%, 1%, and 15% respectively, and that any correlations among the errors, most notably between $\overline{n}_e$ and $P_{L,th}$, are ignored. ITER gives the ratio of λ_{ITER} to STD, where λ_{ITER} is the distance between the design point of ITER and the database average of the variables (ln(RGEO), etc.) along the corresponding p.c. direction. As was derived in [7], the value, ITER, is

Variable	$ln(RGEO)$	$ln(R/a)$	$ln(IP)$	$ln(BT)$	$ln(MEFF)$	$ln(NEL)$	$ln(KAPPA)$	$ln(PLTH)$
$ln(RGEO)$	1.00							
$ln(R/a)$	-0.42	1.00						
$ln(IP)$	**0.72**	**-0.81**	1.00					
$ln(BT)$	0.42	-0.38	0.64	1.00				
$ln(MEFF)$	-0.08	-0.31	0.15	-0.04	1.00			
$ln(NEL)$	-0.33	-0.10	0.17	0.33	0.12	1.00		
$ln(KAPPA)$	-0.23	-0.31	0.16	-0.30	0.21	0.19	1.00	
$ln(PLTH)$	0.68	-0.56	**0.79**	0.68	-0.11	0.19	-0.11	1.00

Table 9: L-mode Plasma Correlation Matrix

important for computing the uncertainty in the confinement time extrapolation to the ITER design point. $ITER > 4$ implies a large uncertainty in the prediction in that direction. The nominal ITER parameters used to compute this latter value are $R = 8.14\ m$, $a = 2.80\ m$ $(R/a = 2.91)$, $I_p = 21\ MA$, $B_T = 5.68\ T$, $M_{eff} = 2.5$, $\overline{n}_e = 1.3 \times 10^{20}\ m^{-3}$, $\kappa = 1.6$, and $P_{L,th} = 192\ MW$.

Approximately 75% of the total variation in the data can be accounted for by the largest principal component, and over 95% in the total variation by the largest four. The values of ITER, which are all ≤ 4 except for the sixth p.c., indicate that the database is reasonably well conditioned for extrapolation to ITER. The sixth p.c. has a complicated dependence on plasma size, shape, density, and toroidal field. Increasing the range of values in each of the p.c.s with values of "ITER" near 4 (p.c. 1, 6, and 7) would lead to a reduction in uncertainty in each of these directions, and, as will be seen in Section 5, a reduction in the uncertainty in the projected $\tau_{E,th}$ for ITER. The database is also well-conditioned with respect to ERR, except for the fifth p.c., which depends most strongly on the plasma's effective mass. This indicates the relatively high uncertainty in the determination of this parameter in the database.

4. Scaling of the Energy Confinement Time

4.1. OH Confinement

As it is generally accepted that the energy confinement in the SOC regime does not depend on $\overline{n}_e$ and I_p, the regression analysis has been performed neglecting these variables. Most of the database consists of data from tokamaks with circular cross section, with the exception of JET, which is elongated, and Alcator C-Mod, also with a significant elongation and triangularity. The regression on the subset containing data from the circular tokamaks (381 observations), assuming a power law form for the scaling, results in:

$$\tau_E = 0.052 M_{eff}^{0.27\pm.04} R^{2.07\pm.03} (R/a)^{-0.74\pm.10} B_T^{0.33\pm.03} \tag{3}$$

with a linear regression coefficient of 0.98 and a Root Mean Square Error of 12.7%. The inclusion of JET and Alcator C-Mod data (617 observations total), including the dependence on κ results in:

$$\tau_E = 0.047 M_{eff}^{0.14\pm.03} R^{2.02\pm.02} (R/a)^{-0.63\pm.08} B_T^{0.35\pm.03} \kappa^{1.34\pm.07} \tag{4}$$

with a regression coefficient of 0.98 and a Root Mean Square Error of 15.2%. The inclusion of κ produces a relevant change only in the dependence of M_{eff}, which is

	$ln(RGEO)$	$ln(R/a)$	$ln(IP)$	$ln(BT)$	$ln(MEFF)$	$ln(NEL)$	$ln(KAPPA)$	$ln(PLTH)$	STD	ERR	ITER
pc1	0.20	-0.12	0.62	0.23	0.00	0.06	0.00	0.71	1.39	0.08	3.78
pc2	0.10	-0.24	0.66	-0.16	0.28	-0.14	0.22	-0.58	0.49	0.18	0.55
pc3	-0.46	-0.05	0.09	0.26	0.15	0.81	0.14	-0.09	0.46	0.11	1.28
pc4	0.15	0.12	0.06	0.82	-0.08	-0.13	-0.38	-0.33	0.31	0.16	2.06
pc5	-0.04	-0.10	-0.21	0.07	0.92	-0.14	-0.21	0.17	0.24	0.42	-1.79
pc6	0.64	0.37	0.04	-0.28	0.12	0.49	-0.33	-0.11	0.19	0.16	4.79
pc7	0.17	0.60	-0.06	0.23	0.19	-0.08	0.72	0.04	0.13	0.15	3.85
pc8	0.52	-0.64	-0.35	0.20	-0.03	0.18	0.34	-0.03	0.08	0.13	0.50

Table 10: Principal Components

somewhat correlated with κ, as can be seen from Table 8. This last regression suggests a strong dependence on κ that does not emerge from the analysis of the data of a single tokamak (e.g., Alcator C-Mod), together with a very small dependence on the ion mass that is also in contradiction with the data from single machines (e.g,. FTU). One reason for this may be that the ohmic data from JET that have been included in the L-mode database essentially as a reference for the heated plasma phases, without the requirement of a stationary plasma condition. As a consequence, the result of the regression for circular tokamak may be more reliable and no definitive conclusion on the dependence from elongation can be drawn.

In Eq. 3 the rather weak dependence on B_T has been observed on other tokamaks (FTU [16], ASDEX [36]) while a somewhat stronger dependence was observed on Tore-Supra [37]. The ohmic data from Tore-Supra in the L-mode database, however, are a very limited representation of the operation space of that tokamak (see Tables 5 and 6).

The ohmic regime can be compared to the L-mode for additionally heated plasmas by using the L-mode energy confinement scaling on the ohmic database. In Figure 1 the comparison is made with ITER89P scaling, showing that at the higher densities the ohmic energy confinement is well reproduced by ITER89P, so that the SOC regime can be considered a standard L-mode plasma. If the L-mode regression of Eq. 8 is considered (see Figure 2), a similar conclusion can be drawn, although at the highest densities the new regression tends to overestimate slightly the energy confinement time. This is due to the stronger density dependence of Eq. 8 compared to ITER89P. A more detailed analysis of the OH data, including use of Z_{eff} as a regressor, will be attempted when this dataset is more complete.

4.2. L-mode Confinement

4.2.1. Comparison With Existing Scaling Expressions

The global confinement times of the L-mode data will be compared with the previously developed ITER89-P scaling in this section. Figure 3 shows the natural logarithms of the experimental total confinement times compared to the predicted values from the ITER89-P scaling. For this comparison, 1798 observations were used (the number for which τ_E is available). The R^2 of the fit is 0.96 with a Root Mean Square Error (RMSE) of 19.1%. The fit is linear with nearly zero offset; the intercept is -0.12, while the slope of the fit is 0.91, indicating a set of slightly lower confinement times than would be given by the scaling. To determine the machine-to-machine variations of the fit, the ratios $(\tau_e/\tau_e^{ITER89-P})$ are plotted as a function

DEVICE	Mean of Residual	Standard Deviation of Residual
Alcator C-Mod	-0.08	0.08
ASDEX	0.13	0.08
DIII	0.01	0.15
DIII-D	-0.11	0.17
JET	0.06	0.13
JFT-2M	0.21	0.17
JT-60	0.03	0.13
PBX-M	0.42	0.09
PDX	-0.05	0.15
T-10	-0.36	0.31
TEXTOR	-0.21	0.14
TFTR	-0.08	0.15
Tore-Supra	-0.28	0.17

Table 11: τ_E-ITER89-P Fit Residuals $(ln(\tau_E) - ln(\tau_E^{ITER89-P}))$

of $ln(RGEO)$ in Fig. 4, and the mean and standard deviations of the residuals $(ln(\tau_e) - ln(\tau_e^{ITER89-P}))$ are given for each machine in Table 11. As can be seen, most prominantly from the table, ASDEX, JFT-2M, and most dramatically PBX-M stand out as having total confinement times significantly greater, in a statistical sense, than those predicted by ITER89-P. PBX-M has an aspect ratio of 5.5, which is outside the range of values typical of the machines whose data were used to develop the scaling. Alcator C-Mod, T-10, TEXTOR, and Tore-Supra, on the other hand, are generally overpredicted by the scaling.

4.2.2. Power Law Scaling of the L-Mode Dataset

Total and thermal energy confinement time scalings of the L-mode dataset will be presented in this section. The simplest approach here will be taken in that a power law form for the scaling is assumed. The form of the scaling, therefore, is:

$$\tau_E = \alpha_c I_p^{\alpha_I} B_T^{\alpha_B} \kappa^{\alpha_\kappa} R^{\alpha_R} (R/a)^{\alpha_A} \overline{n}_e^{\alpha_n} M_{eff}^{\alpha_M} P^{\alpha_P} \tag{5}$$

For the total τ_E scaling, PL (see appendix) is chosen as the power regressor variable. The estimates of the parameters, α_i, and their standard errors are given in the third and fourth columns of Table 12, and the experimental τ_E plotted as a function of the fitted values are plotted in Fig. 5. The fit is given in units of in units of MA, m, m, -, 10^{19} m^{-3}, T, AMU, *and* MW. The fit has $R^2 = 0.96$ and an

Variable	ITER89-P Value	New Estimate	Standard Error	Estimate ($WFFORM/WTOT \leq 0.4$)
Constant	0.038	0.037	0.002	0.029
I_p	0.85	0.74	0.02	0.91
B_T	0.20	0.20	0.02	0.08
κ	0.5	0.67	0.03	0.65
R	1.5	1.69	0.03	1.58
(R/a)	-0.3	-0.31	0.04	0.09
$\overline{n}_e$	0.1	0.24	0.02	0.24
M_{eff}	0.5	0.26	0.02	0.22
P	-0.5	-0.57	0.01	-0.59

Table 12: τ_E scaling parameters

$RMSE = 17.3\%$. The parametric trends of this L-mode scaling are similar to those of ITER89-P (see second column). There is a slightly weaker dependence on plasma current in the new scaling, but a stronger dependence on plasma size, shape, and density, and a slightly stronger degradation with heating power. One difference between the ITER89-P and this new scaling is that while both the M_{eff} and κ dependence was fixed at $M_{eff}^{0.5}$ and $\kappa^{0.5}$ for ITER89-P, M_{eff} and κ were treated as a free regressor variables here.

The mean and standard deviations of the residuals, grouped by device, are given in Table 13. PBX-M stands out as being underpredicted by the model (residual mean $\gg$ residual std. dev.), perhaps indicating that high aspect ratio, or very strong shaping, is still not properly being taken into account. TEXTOR and Tore-Supra are slightly overpredicted by the scaling.

The third and fourth columns of Table 12 give the parameter estimates for the full subset of 1798 observations, irrespective of the relative thermal to fast particle energy content (similar to the ITER89-P scaling). The effect of the fast particle energy content on the scaling can be examined by further constraining this data subset such that the fast ion content (due to RF or NBI) is $\leq 40\%$ ($WFFORM/WTOT \leq 0.40$), as was done for the standard subset of the H-mode database. This eliminates 637 observations, dominated by DIII and JT-60 for which WFFORM is not available. The scaling parameters with this constraint included are given in the fifth column of Table 12. For this fit, $R^2 = 0.98$ and $RMSE = 16.0\%$, which is slightly better than the standard fit. As can be seen, the fit with this additional constraint shows significant differences from the standard fit, most notably in the I_p scaling, which is stronger, and in the aspect ratio scaling, which now shows a slightly positive instead of a negative dependence.

The $\tau_{E,th}$ scaling parameter estimates and their standard errors for the 1312 obser-

DEVICE	Mean of Residual	Standard Deviation of Residual
Alcator C-Mod	0.02	0.09
ASDEX	0.07	0.11
DIII	-0.02	0.14
DIII-D	-0.09	0.20
JET	0.04	0.10
JFT-2M	0.11	0.15
JT-60	0.00	0.15
PBX-M	0.40	0.09
PDX	0.01	0.18
T-10	-0.24	0.28
TEXTOR	-0.18	0.13
TFTR	0.03	0.19
Tore-Supra	-0.17	0.10

Table 13: τ_E Fit Residuals

vations in the standard L-mode dataset (see Sec. 3.1) are given in the second and third columns of Table 14 (the values in the last two columns will be discussed shortly). A plot of the fit is shown in Fig. 6. For this fit, $R^2 = 0.97$ and the $RMSE = 15.8\%$. As can be seen in Table 14, the size dependence of the thermal confinement is almost all contained in the major radius, R, and the scaling with plasma current is stronger than that in τ_E scaling (note that the B_T scaling is weaker), and is almost linear. Other differences between the τ_E and $\tau_{E,th}$ scalings are the much stronger density dependence and degradation with heating power seen in the $\tau_{E,th}$ scaling. Note that PLTH (see appendix) is used for the $\tau_{E,th}$ scaling. Radiation losses are not subtracted from either PL or PLTH, consistent with the H-mode analysis methodology. The thermal confinement scaling for this L-mode data subset is nearly perfectly Bohm-like, as compared to the ITER93H expression which was nearly perfectly high-β, and very close to gyroBohm [8]. As can be seen from the residual statistics presented in Table 15, PBX-M is underpredicted by the scaling, with none of the other machines residuals showing any statistically significant offset from zero. The fit to the data, performed with the engineering variables but expressed in physics variables, satisfies the Kadomtsev (high-β) constraint, and is given by

$$\tau_{E,th} B \propto \rho_*^{-1.98} \nu_*^{0.19} \beta_t^{-1.39} (R/a)^{4.26} \kappa^{0.87} M_{eff}^{0.74} q^{0.14} \tag{6}$$

where $\rho_* \propto \sqrt{\frac{(a/R)P\tau}{a^3 n_e I^2 \kappa}}$ and $\nu_* \propto \frac{a^7 n_e^3 \kappa^2}{(a/R)^3 (P\tau)^2}$. The standard subset of the L-mode

confinement can be examined for further additional dependences that may depend on either plasma configuration or type of auxiliary heating. Constraining this data subset by the additional fast ion energy constraint, as discussed for the τ_E fit, produces essentially no change in the scaling coefficients to within approximately one standard error. As mentioned previously, and as shown in Table 3, 861 of the discharges are limited while the remaining 451 are diverted. The criterion that the discharges be limited eliminate most of the DIII-D, JFT-2M, and JT-60 discharges, and all of the ASDEX and PBX-M discharges. The thermal confinement scaling exponents, based solely on the 861 limiter discharges, are given in the fourth column of Table 14. As can be seen from the values in the table, there are slight modifications to the κ, R, and density scaling coefficients, with the largest differences occuring in the R/a and M_{eff} dependence. The loss of the high aspect ratio PBX-M data in the limiter dataset compromises the ability to determine the aspect ratio dependence, as discussed in the H-mode database work [7]. Interestingly, there is no dependence of effective mass in this limiter-only dataset; this result has been reported by TFTR based on dedicated isotopic mass dependence experiments [33]. When applied to the entire 1312 entry L-mode standard subset, the limiter-only thermal scaling yields a fit characterized by an $R^2 = 0.97$ (comparable to the full fit), and an $RMSE = 17.6\%$, which is greater than that of the full fit (15%).

In general, the limiter-only scaling predicts well the confinement times for the 451 observation divertor-only subset. The mean residual of the divertor subset $(ln(\tau_{E,th}) - ln(\tau_{E,th}^{scaling}))$ is -0.07 (slightly overpredicting divertor confinement), but the standard deviation of the residual is larger than the mean, at 0.22. A breakdown by machine indicates that the $\tau_{E,th}$s of diverted Alcator C-Mod and DIII-D observations are overpredicted by the limiter-only scaling, both with a mean residual of -0.25 and standard deviations of 0.04 and 0.16 respectively. PBX-M is underpredicted by the scaling, with a mean residual of 0.40 and a standard deviation of 0.08. The rest of the divertor observations are well predicted by the limiter-only scaling.

The next comparison that can be made is to break up the discharges into ion and electron preferential heating, in this case ignoring any limiter vs. divertor differences. Classifying the discharges as ion or electron preferential can be somewhat problematic owing to uncertainties in the various RF scenarios. In order to classify a discharge as electron preferential, the following criterion was used: $\frac{POHM+PICRHC+PECHC+PLHC}{P_{tot}} > 0.5$, where $PICRHC$ in the numerator assumes that the ICRH heats the electrons, and where the denominator includes the contribution from neutral beam heating. The 49 LH heating entries of Tore-Supra and the 20 ECRH entries of T-10 are clearly electron preferential. The discharges on JET and TEXTOR that satisfy the above

Variable	Estimate	Standard Error	Limiter Only Estimate	Ion Heating Only Estimate
Constant	0.023	0.001	0.044	0.024
I_p	0.96	0.02	0.95	1.00
B_T	0.03	0.02	0.05	0.00
κ	0.64	0.03	0.75	0.61
R	1.83	0.03	1.68	1.76
(R/a)	0.06	0.04	-0.22	0.13
$\overline{n}_e$	0.40	0.02	0.30	0.36
M_{eff}	0.20	0.02	-0.01	0.23
P	-0.73	0.01	-0.74	-0.73

Table 14: $\tau_{E,th}$ scaling parameters

criterion account for a total of 216 entries. The Alcator C-Mod RF discharges are more difficult to classify, although not much difference in the resulting scalings was seen with the 55 C-Mod entries being classified as ion or electron preferential. This is possibly due to the strong coupling between the two thermal species in the relatively high density operation regime of C-Mod. Consequently, the C-Mod discharges will be treated as being ion preferential.

The results of the fit for the ion heating only discharges are shown in Table 14 in the fifth column. As can be seen from the table, there appears to be little effect on the overall $\tau_{E,th}$ scaling when the dataset is restricted to ion heating only. The most significant change occurs in the exponents for the major radius and aspect ratio. The ion heating only scaling describes the electron heating discharges well, with an overall mean residual of -0.02 for the scaling (slightly overestimating $\tau_{E,th}$); however, the standard deviation of the residuals is 0.14, indicating that any offset is well within statistical uncertainty. The same conclusion holds on a machine-to-machine basis. When applied to the full 1312 L-mode dataset, the scaling yields $R^2 = 0.97$ and $RMSE = 16.0\%$, indicating an almost identical statistical fit to the data as the full scaling. The conclusion to be drawn from this is that the type of heating does not introduce differences in the L-mode scaling trends.

4.2.3. Relation to the H-modes

The L-mode thermal confinement time scaling expression presented in the previous section is somewhat similar to both the ELM-free and ELMy H-mode thermal confinement scaling. Comparisons of the leading coefficient and exponents of the L-mode scaling with both the ELM-free [38, 8] and ELMy [39] H-mode scalings are shown in Table 16.

The ELMy and ELM-free standard H-mode datasets will be compared with the

DEVICE	Mean of Residual	Standard Deviation of Residual
Alcator C-Mod	-0.03	0.09
ASDEX	-0.03	0.09
DIII-D	-0.04	0.20
JET	0.02	0.12
JFT-2M	0.02	0.19
JT-60	0.01	0.14
PBX-M	0.25	0.09
PDX	0.08	0.19
T-10	0.03	0.27
TEXTOR	-0.01	0.08
TFTR	-0.05	0.18
Tore-Supra	0.01	0.09

Table 15: $\tau_{E,th}$ Fit Residuals

Parameter	L-Mode	Elm-free H	ELMy H
$Constant$	0.023	0.036	0.034
I_p	0.96	1.06	0.90
B_T	0.03	0.32	0.05
κ	0.64	0.66	0.80
R	1.83	1.79	2.10
R/a	0.06	0.11	-0.20
M_{eff}	0.20	0.41	0.40
$\overline{n}_e$	0.40	0.17	0.30
P	-0.73	-0.67	-0.65

Table 16: Comparison of L- and H-Mode $\tau_{E,th}$ scaling parameters

L-mode $\tau_{E,th}$ scaling here. The overall fit to the ELMy dataset is shown in Fig. 7. The fit has a mean $\tau_{E,th}/\tau_{E,th,L}$ of 1.38, and a standard deviation (of this ratio) of 0.33 (note that this is less than a 40% increase in thermal energy confinement time going from L- to H-mode). A closer examination on a machine-to-machine basis reveals a systematic trend, however. Fig. 8 shows the mean and standard deviation of the above confinement time ratio, indicating an increasing H-mode enhancement factor with increasing machine size (or decreasing aspect ratio), reaching an average value of approximately 2 for JET. This tendency could also be seen from a plot of the fusion triple product against the stored magnetic field energy in L- and H-modes [40]. The enhancement factor is also seen to generally increase with decreasing average ρ_* when plotted against this variable. While there is much scatter in the data, the trend is obvious for the dataset as a whole, with the exception of the high-β PBX-M discharges, which show an increasing enhancement factor with increasing ρ_*.

The ELM-free results are shown in Fig. 9. The mean $\tau_{E,th}/\tau_{E,th,L}$ is greater than in the ELMy case, with a value of 1.67 and a standard deviation of this ratio of 0.48. The machine-to-machine analysis (Fig. 10) reveals a trend similar to that found for the ELMy dataset, with an increasing enhancement factor with increasing size (or decreasing aspect ratio). For JET, the average enhancement factor is 2.15. It was noted earlier that the L-mode scaling underpredicted the high aspect ratio and highly shaped PBX-M data. This is the opposite to the trends reflected in the H-mode data (perhaps related to the fact that the PBX-M L- to H-mode confinement enhancement was not as great as on other devices). The trend of increasing enhancement factor with decreasing ρ_* is seen also in the ELM-free data.

5. Discussion and Extrapolation to ITER

In this article, a discussion of the L-mode database that was compiled over the last several years under the auspices of what is now the ITER Confinement Database and Modeling Working Group was presented. This effort was the first of its kind to compile the appropriate type and amount of data necessary to develop thermal confinement scalings for L-mode plasmas. The compilation constituted a major effort and involved the cooperation between colleagues from many fusion laboratories. The approach that was taken, and the data that were included, followed closely those of earlier H-mode database efforts, and it has resulted in an L-mode database that is much more comprehensive than any L-mode database put together in the past.

The database consists of 2938 entries from 14 different tokamaks, and it ranges from OH only to RF and NBI auxiliary heating. Both limiter and divertor discharges

are represented, although both configurations fit the resulting scalings equally well. The L-mode scalings developed from the data subsets (no He discharges included in the fits) are:

$$\tau_E = 0.037 I_p^{0.74} B_T^{0.20} \kappa^{0.67} R^{1.69} (R/a)^{-0.31} \overline{n}_e^{0.24} M_{eff}^{0.26} P^{-0.57} \tag{7}$$

and

$$\tau_{th} = 0.023 I_p^{0.96} B_T^{0.03} \kappa^{0.64} R^{1.83} (R/a)^{0.06} \overline{n}_e^{0.40} M_{eff}^{0.20} P^{-0.73} \tag{8}$$

in units of sec, MA, m, m, -, $10^{19}\ m^{-3}$, T, AMU, MW.

The last issue remaining is the extrapolation to ITER. For the nominal ITER parameters: $R = 8.14\ m$, $a = 2.80\ m$ $(R/a = 2.91)$, $I_p = 21\ MA$, $B_T = 5.68\ T$, $M_{eff} = 2.5$, $\overline{n}_e = 1.3 \times 10^{20}\ m^{-3}$, $\kappa = 1.6$, and $P_{L,th} = 192\ MW$, the thermal confinement time is 2.2 sec. (The confinement time predicted from ITER89-P for comparison is 2.3 sec). The thermal confinement time during the pre-transition L-phase, with $< n_e >= 5 \times 10^{19}\ m^{-3}$ and $P_{heat} = 100\ MW$, is estimated to be 2.4 sec. An estimate of the uncertainty of the extrapolation is given in an estimated 95% confidence interval, which can be expressed as [7]

$$\frac{\delta \tau_{E,th}}{\tau_{E,th}} = \pm \frac{2 c_s \sigma}{N^{1/2}} [1 + \sum_i (ITER_i^2)]^{1/2} \tag{9}$$

where the values, $ITER_i$, are given in Table 10, σ is the standard deviation of the fit, and N is the number of points in the fit. The constant c_s reflects the sources of scatter in the data. $c_s = 1$ characterizes the restrictive assumption that a single simple power law holds for all machines, and that all major factors influencing the confinement time are included in the regression formula. This implies that the residual scatter in the data can be viewed as independent variations. Because of correlated groups of data and sources of systematic variations that are not covered by the scaling, we choose $c_s = 3$. This choice is larger than that for the H-mode confinement time extrapolation, where $c_s = 2$ was used, since the L-mode sample size is larger than that of the H-mode database and the relative influence of the systematic variation increases with sample size. For the thermal confinement time scaling, $\sigma = 0.158$, $N = 1312$, and $\sum_i (ITER_i^2) = 61.7$, giving $\delta \tau_{E,th} = \pm 0.5 sec$. The minimum required confinement time for ITER to ignite is 5.6 sec.; for $\tau_{E,th} = 2.2\ sec$, this means a required H-mode enhancement factor of approximately 2.6 relative to the new L-mode thermal confinement scaling. Such an enhancement factor may be achievable for ITER operation in the ELMy H-mode, as the scalings derived earlier

imply a systematic increase of this factor with increasing machine size (or decreasing ρ_*).

The most important enhancement to the L-mode database, as far as the projections to ITER are concerned, is one that would reduce the uncertainty in the confinement prediction. To this end, the "ITER" values of the various principal components (see Table 10) give some guidance. As discussed earlier, values of $ITER > 4$ imply a large uncertainty in the prediction in that direction, and, therefore, increase the uncertainty in the τ_E prediction (see Eq. 9). In order to reduce the values of ITER, it would be necessary to increase the range of data in these principal component directions, and this can be accomplished by either performing experiments at low and high values of these p.c.s, or by having all the machines perform complete parameter scans in their accessible operating space (including isotope scaling). Furthermore, it would be important to reduce the systematic uncertainty in parameters from which the scaling variables are derived, parameters such as, for example, $W_{thermal}$, P_{bo}, and P_{cx}.

The L-mode database, ITERLDB.1, can be found on the ftp server at PPPL (ftp.pppl.gov) by logging in as ANONYMOUS, and moving to the /pub/Lmode directory.

Appendix A. Database variable name translation table

Variable	Database Variable Name
a	AMIN
R	RGEO
I_p	IP
B_T	BT
κ	KAPPA
δ	DELTA
q_{95}	Q95
q_{edge}	QEDGE
$\overline{n}_e$	NEL
M_{eff}	MEFF
Z_{eff}	ZEFF
W_{tot}	WTOT
P_{oh}	POHM
P_{nbi}	PNBI
P_{ecrh}	PECRHC
P_{icrh}	PICRHC
P_L	PL
$P_{L,th}$	PLTH
P_{rad}	PRAD
τ_E	TAUE
$\tau_{E,th}$	TAUTH

Appendix B. List of variables for ITERLDB.1 L-mode confinement database

General

1. **TOK:** This variable designates which tokamak has supplied the data. Possible values are: CMOD (Alcator C-Mod), ASDEX, D3D (DIII-D), DIII, FTU, JET, JFT2M, JT60, PBXM, PDX, T10 (T-10), TXTR (TEXTOR), TFTR, or TSUPRA (Tore-Supra).

2. **SHOT:** The shot from which the data are taken.

3. **TIME:** Time during the shot at which the data are taken in seconds.

4. **UPDATE:** The date of the most recent update for any variable listed in the database. The format is YYMMDD (Year-Month-Day).

5. **DATE:** The date the shot was taken. The format is YYMMDD.

6. **AUXHEAT:** Type of auxiliary heating. Possible values are:
   NONE : No Auxiliary heating
   NB : Neutral Beam Injection
   IC : Ion Cyclotron Resonance Heating
   EC : Electron Cyclotron Resonance Heating
   NBIC : Combined NBI + IC
   LH : Lower Hybrid Heating
   LHIC : Combined LH + IC

7. **PHASE:** The phase of the discharge at TIME. Possible values are:
   OHM : Ohmic
   L : L-mode
   EP : Enhanced Performance
   LHEP : Lower Hybrid Enhanced Performance
   I : I-Mode

8. **OLTIME:** The start time of the auxiliary heating in seconds.

9. **AUXTIME:** The time of the last change in auxiliary heating power in seconds.

Plasma composition

10. **PGASA:** Mass number of the plasma working gas (AMU).

11. **PGASZ:** Charge number of the plasma working gas.

12. **BGASA:** Mass number of the neutral beam gas (AMU)

13. **BGASZ:** Charge number of the neutral beam gas.

14. **PGASMA:** Mass number of the minority working gas (AMU).

15. **PGASMZ:** Charge number of the minority working gas.

16. **PELLET:** Pellet material if a pellet(s) has been injected.

17. **MEFF:** Effective atomic mass in AMU.

Geometry

18. **RGEO:** The plasma geometrical major radius in meters.

19. **AMIN:** The horizontal plasma minor radius in meters.

20. **KAPPA:** The elongation of the plasma boundary at the separatrix (95% flux surface for PBX-M).

21. **DELTA:** The triangularity of the plasma boundary at the separatrix (95% flux surface for PBX-M).

22. **INDENT:** The indentation of the plasma boundary at the separatrix (95% flux surface for PBX-M).

23. **AREA:** Area of plasma cross section in m^2.

24. **VOL:** The plasmas volume in m^3.

25. **CONFIG:** The plasma configuration. Possible values are: LIM for limiter, IN for inside limiter, OUT for outside limiter, SN for single null, SNO for outside single null, SNL for lower single null, DN for double null, or EDIV for ergodic divertor.

26. **IGRADB:** Indicates when CONFIG = SN whether the ion ∇B drift is towards (1) or pointing away from (-1) the X-point.

27. **XINV:** Sawtooth inversion radius (in units of r/a).

Machine condition

28. **WALMAT:** The material of the vessel wall with possible values SS for stainless steel, IN for inconel, C for carbon, IN/C for inconel with carbon, CSS for (partly) carbon on stainless steel, Mo for molybdenum, BORO for boron, and TMBA for boron + carbon.

29. **LIMMAT:** The material of the limiters (see above).

30. **DIVMAT:** The material of the divertor tiles (see WALMAT).

31. **EVAP:** The evaporated material used to cover the inside of the vessel with possible values BO, BOROA (B2H6 + CH4 + H2) or BOROB (B2H6 + H2, BOROC (B2H6 + He), and BOROD (B2H6 + He + D2) for boron, C, or CARBH (CH4 + D2) for carbon, Si for silicon, TI for titanium, and NONE for no evaporation.

Magnetics

32. **BT:** The vacuum toroidal magnetic field at RGEO in Tesla. Negative values indicate operation with reversed toroidal field.

33. **IP:** The plasma current in Amperes. Negative values are possible.

34. **VSURF:** The loop voltage at the plasma boundary in Volts.

35. **Q95:** The plasma safety factor from an MHD equilibrium fit evaluated at the 95% flux surface.

36. **QEDGE:** The plasma safety factor determined from the ITER q-scaling expression.

37. **BEPMHD:** Poloidal beta computed from MHD.

38. **BEPDIA:** Poloidal diamagnetic beta.

39. **BETMHD:** Toroidal beta computed from MHD.

40. **BEIMHD:** Beta Shafranov from MHD.

41. **BEILI2:** Poloidal beta plus $l_i/2$ determined from MHD or probe measurements.

Densities

42. **NEL:** Central line average electron density in m^{-3}.

43. **DNELDT:** The time rate of change of NEL in m^{-3}/s.

44. **NEV:** The volume averaged electron density in m^{-3}.

45. **NE0:** The central electron density at the magnetic axis in m^{-3}.

Impurities

46. **ZEFF:** Line average plasma effective charge.

47. **PRAD:** Total radiated power in Watts.

Input Powers

48. **POHM:** Total ohmic power in Watts.

49. **ENBI:** Neutral beam energy weighted by power in Volts. This quantity is calculated from $\Sigma E_i P_i / \Sigma P_i$ where E_i is the beam energy for source i and P_i is the beam power for source i.

50. **PINJ:** Total injected neutral beam power that passes into the torus in Watts.

51. **BSOURCE:** The power fractions injected by neutral beam. e.g., if P1 = 80%, P2 = 10% and P3=10% then BSOURCE = 801010.

52. **PINJ2:** The injected neutral beam power from a second source BSOURCE2 in Watts. Zero if no beams of second source are on.

53. **BSOURCE2:** The power fractions injected by neutral beam with the second source.

54. **PNBI:** Total injected neutral beam power minus shine through in Watts. Zero if no beams are on.

55. **PFLOSS:** Amount of neutral beam power in Watts that is lost from the plasma through charge exchange and unconfined orbits.

56. **ICFREQ:** Frequency of ICRH waves in Hz.

57. **ICSCHEME:** ICRH heating scheme. Possible Values: HMIN for H minority, HE3MIN for 3He minority and FWEH for Fast Wave Electron Heating.

58. **PICRHC:** ICRH power in Watts coupled to the plasma. Zero if no ICRH is applied.

59. **ECHFREQ:** ECRH frequency in Hz.

60. **ECHLOC:** Location of ECRH launch, IN identifies waves launched from the high field side or inside of the vessel and OUT is from the low field side.

61. **PECHC:** ECRH power in Watts coupled to the plasma. Zero if no ECRH is applied.

62. **LHFREQ:** LH frequency in Hz.

63. **LHNPAR:** Peak $n_{\parallel}$ of injected LH waves.

64. **PLHC:** LH power in Watts coupled to the plasma. Zero if no LH is applied.

65. **DWDIA:** Time rate of change of the total plasma stored energy as determined by the diamagnetic loop in Watts.

66. **DWMHD:** Time rate of change of the total plasma stored energy as determined from MHD in Watts.

67. **PTOT:** Estimated total heating power in Watts corrected for neither dW/dt nor fast particle losses.

68. **PL:** Estimated total heating power in Watts corrected for dW/dt but not for charge exchange, unconfined orbit losses, or radiated power. Radiated power was not available for all observations.

69. **PLTH:** Estimated total heating power in Watts corrected for dW/dt and for charge exchange and unconfined orbit losses, but not for radiated power. Radiated power was not available for all observations.

Temperatures

70. **TEV:** The volume averaged electron temperature eV.

71. **TE0:** The electron temperature at the magnetic axis in eV.

72. **TIV:** The volume averaged ion temperature in eV.

73. **TI0:** The ion temperature at the magnetic axis in eV.

Energies

74. **WDIA:** Total plasma energy in Joules as determined from the diamagnetic loop.

75. **WMHD**: Total plasma energy in Joules as determined by a MHD equilibrium fit.

76. **WTOT:** Preferred total plasma energy in Joules.

77. **WEKIN:** Total thermal electron plasma energy in Joules as determined from kinetic measurements.

78. **WIKIN:** Total thermal ion plasma energy in Joules as determined from kinetic measurements.

79. **WKIN:** Total thermal plasma energy in Joules as determined from kinetic measurements.

80. **WTH:** Estimated thermal plasma energy content (preferred) in Joules.

81. **WFPER:** Total perpendicular fast ion energy due to NBI in Joules as determined from transport calculations.

82. **WFPAR:** Total parallel fast ion energy due to NBI in Joules as determined from transport calculations.

83. **WFFORM:** Total fast ion energy due to NBI in Joules estimated from approximate formula (WFPER + WFPAR). Zero if no NBI is applied.

84. **WFANI**: Estimate of fraction of perpendicular fast ion energy as compared to the total fast ion energy due to NBI. If WFPER and WFPAR are available WFANI = WFPER/(WFPER + WFPAR).

85. **WFICRH:** Estimate of the perpendicular fast ion energy content during ICRH heating in Joules.

86. **WFICRHP:** Estimate of the parallel fast ion energy content during ICRH heating in Joules.

87. **WFANIIC:** Estimate of fraction of perpendicular fast ion energy as compared to the total fast ion energy due to ICRH.

Energy confinement times

88. **TAUMHD:** Total MHD energy confinement time (WMHD/(POHM + PNBI + PICRHC + PECHC + PLHC - DWMHD)) in seconds.

89. **TAUDIA:** Total diamagnetic energy confinement time (WDIA/(POHM + PNBI + PICRHC + PECHC + PLHC - DWDIA)) in seconds.

90. **TAUE:** Estimated total energy confinement time (WTOT/PL) in seconds.

91. **TAUTOT:** Estimated total energy confinement time (WTOT/PLTH) in seconds.

92. **TAUTH:** Estimated thermal energy confinement time (WTH/PLTH) in seconds.

93. **SELDB1:** Flagging variable for total confinement data analysis (1 if in subset, 0 otherwise).

94. **SELDB2:** Flagging variable for thermal confinement data analysis (1 if in subset, 0 otherwise).

95. **SELDB:** Flagging variable for the standard constraints.

$$SELDB = \sum_{n=1}^{3} a(n) \times 10^{3-n} \qquad \text{(B1)}$$

a(1)=1 if PHASE = L
a(2)=1 if PGASA $<$ 4 and BGASA $<$ 4
a(3)=1 if TAUTH $\neq$ NULL

ACKNOWLEDGEMENTS

This work was supported by US Department of Energy Contract DE-AC02-CHO3073 at the Princeton Plasma Physics Laboratory, DE-AC03-89ER5114 at General Atomics, and DE-AC02-78ET51013 at MIT.

References

[1] GOLDSTON, R., Plasma Phys. Controlled Fusion **26** (1984) 87.

[2] KAYE, S. and GOLDSTON, R., Nucl. Fusion **25** (1985) 65.

[3] YUSHMANOV, P., TAKIZUKA, T., RIEDEL, K., and ET AL., Nucl. Fusion **30** (1990) 1999.

[4] KAYE, S., Phys. Fluids **28** (1985) 2327.

[5] KAYE, S., Phys. Fluids B **2** (1990) 2926.

[6] WAGNER, F., BESSENRODT-WEBERPALS, M., FAHRBACH, H., and ET AL., Isotope dependence of ohmic discharge parameters of ASDEX, in *Controlled Fusion and Plasma Physics*, volume 13B, p. 195, European Physical Society, (Proc. 16th Eur. Conf. Venice, 1989), 1989, Part I.

[7] CHRISTIANSEN, J., CORDEY, J., THOMSEN, K., and ET AL., Nucl. Fusion **32** (1992) 291.

[8] ITER H-MODE DATABASE WORKING GROUP, Nucl. Fusion **34** (1994) 131.

[9] GREENWALD, M., BOIVIN, R., BOMBARDA, F., and ET AL., Phys. Plasmas **6** (1995) 2308.

[10] HAMMETT, G., COLESTOCK, P., GAMMEL, G., and ET AL., Comparison of bouce-averaged quasilinear theory with charge exchange measurements during minority fundamental and majority second harmonic ICRF heating in plt, in *Radio Frequency Plasma Heating*, p. 67, NY, NY, 1985, American Institute of Physics, (Proc. 6th Topical Conf. Callaway Gardens, Ga., 1985).

[11] STROTH, U., KAISER, M., RYTER, F., and ET AL., Nucl. Fusion **35** (1995) 131.

[12] BURRELL, K. and ET AL., Comparisons of energy confinement in Doublet III limiter and divertor discharges with ohmic, nuetral beam, and electron cyclotron heating, in *Plasma Phys. Cont. Nuclear Fusion Research*, volume 1, p. 131, Vienna, Austria, 1985, IAEA, (Proc. 10th Int. Conf. London, 1984).

[13] DEBOO, J., BURRELL, K., EJIMA, S., and ET AL., Nucl. Fusion **26** (1986) 211.

[14] SCHISSEL, D., BURRELL, K., DEBOO, J., and ET AL., Nucl. Fusion **29** (1989) 185.

[15] ANDREANI, R. and ET AL., The Frascati Tokamak Upgrade:, electrical, mechanical, and thermal features, in *Fusion Technology*, volume 1, p. 218, Amsterdam, Netherlands, 1990, North-Holland, (Proc. 16th Symposium, London, 1994).

[16] ALLADIO, F., APICELLA, M., APRUZZESE, G., and ET AL., Energy confinement in FTU ohmic plasmas, in *Plasma Phys. Cont. Nuclear Fusion Research*, volume 2, p. 23, Vienna, Austria, 1995, IAEA, (Proc. 15th Int. Conf. Seville, 1994).

[17] The JET Team, JET latest results and future prospects, in *Plasma Phys. Cont. Nuclear Fusion Research*, volume 1, p. 31, Vienna, Austria, 1987, IAEA, (Proc. 11th Int. Conf. Kyoto, 1986).

[18] J.G. CORDEY, D. B., BHATNAGER, V., BICKERTON, R., BURES, M., and ET AL., Energy confinement with ohmic and strong auxiliary heating, in *Plasma Phys. Cont. Nuclear Fusion Research*, volume 1, p. 99, Vienna, Austria, 1987, IAEA, (Proc. 11th Int. Conf. Kyoto, 1986).

[19] F. RYTER AND THE H-MODE DATABASE WORKING GROUP, Plasma Phys. Controlled Fusion **38** (1996) 1279.

[20] MATSUMOTO, H., FUNAHASHI, A., HASEGAWA, M., and ET AL., Studies of H-mode in the limiter discharges on JFT-2M tokamak, in *Controlled Fusion and Plasma Physics*, volume 11D, p. 5, European Physical Society, (Proc. 14th Eur. Conf. Madrid, 1987), 1987, Part I.

[21] KIKUCHI, M., KIKUCHI, K., AOYAGI, T., and ET AL., Kinetic database of the JT-60 tokamak during 1985-1987 experiments, JAERI Report JAERI-M 91-057, 1991.

[22] SHIRAI, H., TAKIZUKA, T., KIKUCHI, M., and ET AL., Non-dimensional transport scaling and its correlation with local transport properties in JT-60U plasmas, in *Plasma Phys. Cont. Nuclear Fusion Research*, volume 1, p. 355, Vienna, Austria, 1995, IAEA, (Proc. 15th Int. Conf. Seville, 1994).

[23] SAUTHOFF, N., ASAKURA, N., BELL, R., and ET. AL., PBX-M Research Program: Approach to second stability, in *Plasma Phys. Cont. Nuclear Fusion*

Research, volume 1, p. 709, Vienna, Austria, 1991, IAEA, (Proc. 13th Int. Conf. Washington D.C., 1990).

[24] MEADE, D., ARUNASALAM, V., BARNES, C., and ET AL., Pdx experimental results, in *Plasma Phys. Cont. Nuclear Fusion Research*, volume 1, p. 665, Vienna, Austria, 1981, IAEA, (Proc. 8th Int. Conf. Brussels, 1980).

[25] KAYE, S., GOLDSTON, R., BELL, M., and ET AL., Nucl. Fusion **24** (1984) 1303.

[26] CHANG, C. and HINTON, F., Phys. Fluids **25** (1982) 1493.

[27] ESIPCHUK, Y. and ET AL., J. Moscow Phys. Society **1** (1991) 119.

[28] ONGENA, J., CONRADS, H., GAIGNEAUX, M., and ET AL., Nucl. Fusion **33** (1993) 283.

[29] JOHNSON, D., SCOTT, S., BARNES, C., and ET AL., Transport studies in high recycling neutral beam heated discharges in TFTR, in *Controlled Fusion and Plasma Heating*, volume 14B, p. 114, European Physical Society, (Proc. 17th Eur. Conf. Amsterdam, 1990), 1990, Part I.

[30] GRISHAM, L., SCOTT, S., GOLDSTON, R., and ET AL., Phys. Rev. Lett. **67** (1991) 66.

[31] SCOTT, S., BARNES, C., MIKKELSEN, D., and ET AL., Nondimensional transport studies in TFTR, in *Plasma Phys. Cont. Nuclear Fusion Research*, volume 3-4, p. 427, Vienna, Austria, 1993, IAEA, (Proc. 14th Int. Conf. Wurzburg, 1992).

[32] PERKINS, F., BARNES, C., JOHNSON, D., and ET AL., Phys. Fluids B **5** (1993) 477.

[33] BARNES, C., SCOTT, S., BELL, M., and ET AL., Phys. Plasmas **3** (1996) 4521.

[34] TOWNER, H. and ET AL., Rev. Sci. Instrum. **63** (1992) 4753.

[35] HOANG, G., GIL, C., JOFFRIN, E., and ET AL., Nucl. Fusion **34** (1994) 75.

[36] MCCARTHY, P., RIEDEL, K., KARDAUN, O., and ET AL., Nucl. Fusion **31** (1991) 1595.

[37] ZOU, X., HOANG, G., COLAS, L., and ET AL., New dimensionless scaling law of global energy confinement in tore- supra for ohmic plasmas, in *Controlled Fusion and Plasma Physics*, volume 14B, p. 41, European Physical Society, (Proc. 17th Eur. Conf. Bournemouth, 1995), 1995, Part I.

[38] D.P. SCHISSEL AND THE ITER H-MODE CONFINEMENT WORKING GROUP, Analysis of the ITER H-mode confinement database, in *Controlled Fusion and Plasma Physics*, volume 17C, p. 103, European Physical Society, (Proc. 20th Eur. Conf. Lisbon, 1993), 1993, Part I.

[39] O. Kardaun and the ITER H-MODE DATABASE WORKING GROUP, ITER: Analysis of the H-mode confinement and threshold databases, in *Plasma Phys. Cont. Nuclear Fusion Research*, volume 3-4, p. 251, Vienna, Austria, 1993, IAEA, (Proc. 14th Int. Conf. Wurzburg, 1992).

[40] KARDAUN, O., KUS, A., and The L-mode Database Working Group, Generalizing regression and discriminant analysis: catastrophe models for plasma confinement and threshold data, in *Computational Statistics XII*, volume I, p. 396, Physica Verlag, (Compstat XIII, Barcelona, 1996), 1996.

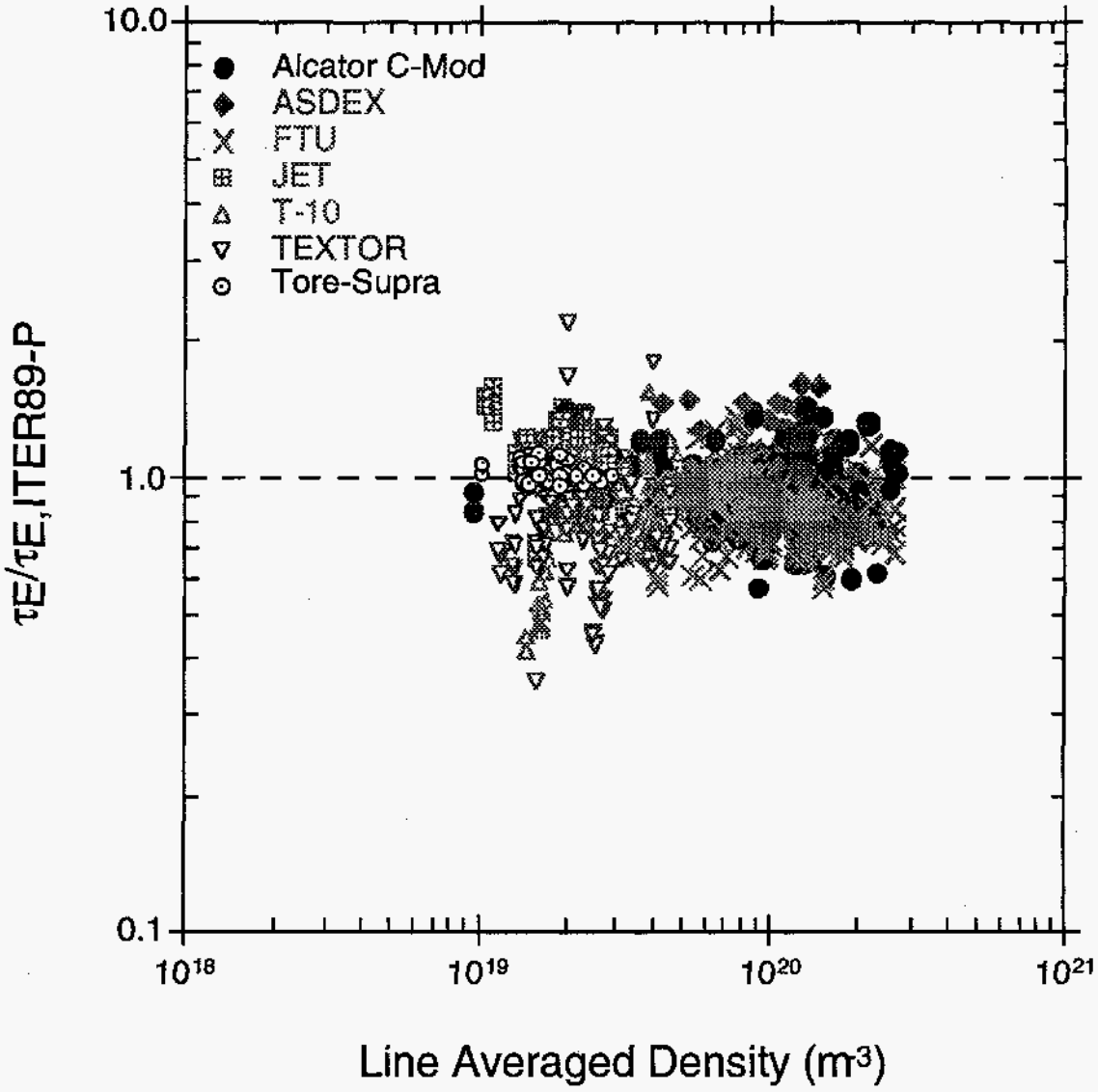

Fig. 1 Ratio between measured energy confinement time and that of the ITER89-P scaling for the deuterium subset of ohmic database versus line averaged density.

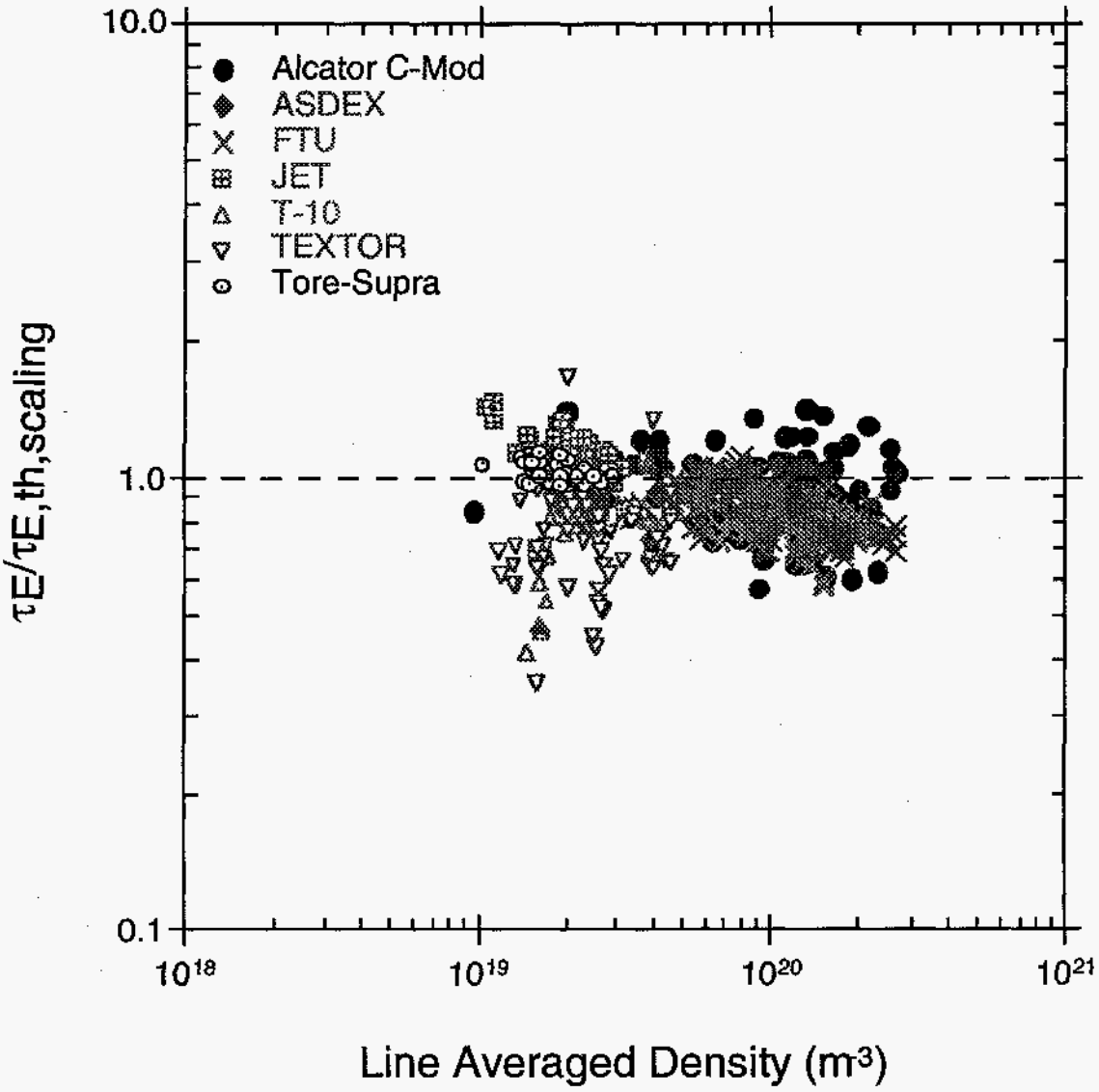

Fig. 2 Ratio between the measured energy confinement time and that of the scaling given in Eq. 8 for the deuterium subset of ohmic database versus line averaged density.

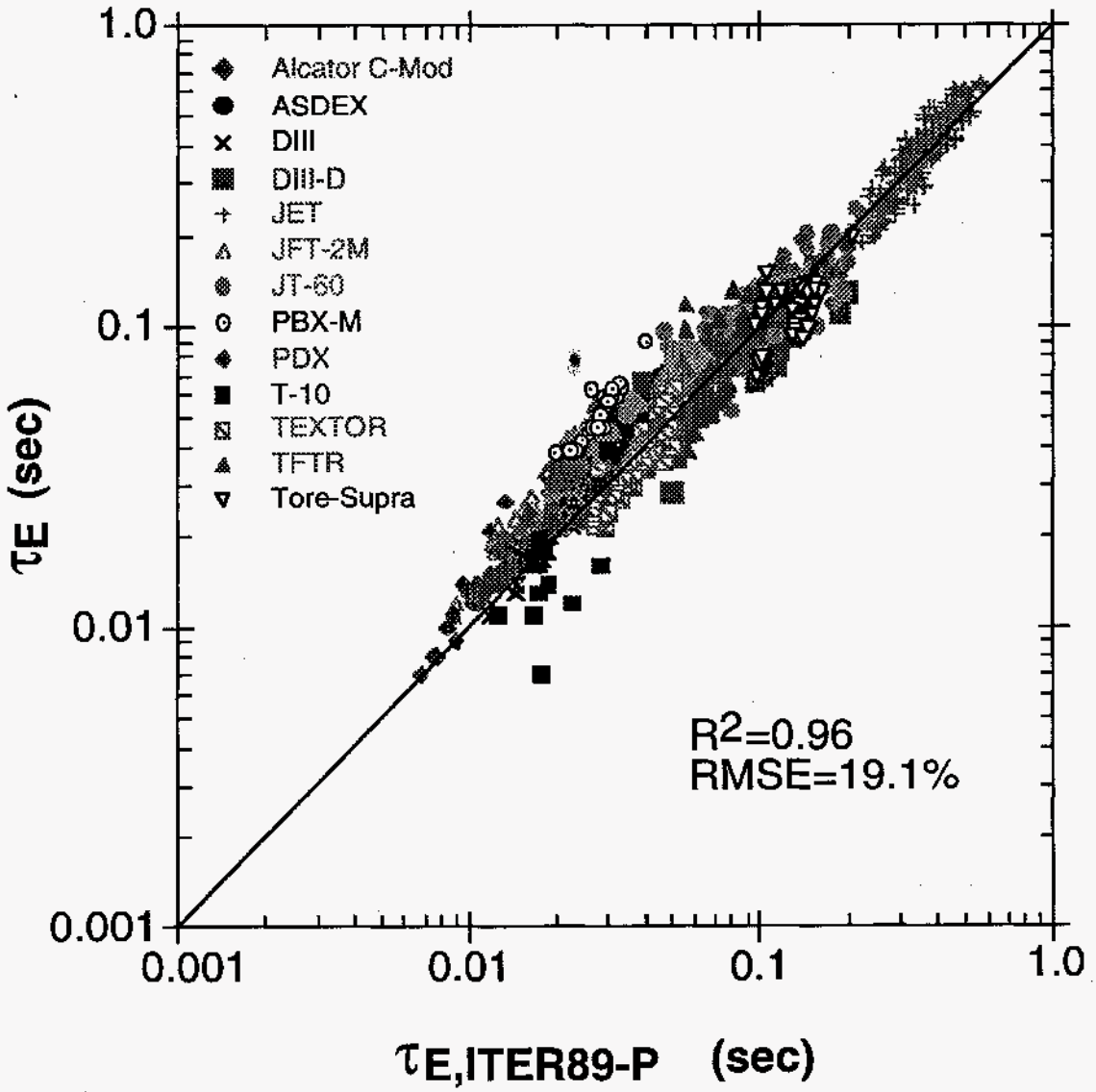

Fig. 3 Total energy confinement time plotted as a function of the ITER89-P scaling. The line corresponds to $\tau_E=\tau_{E,ITER89P}$.

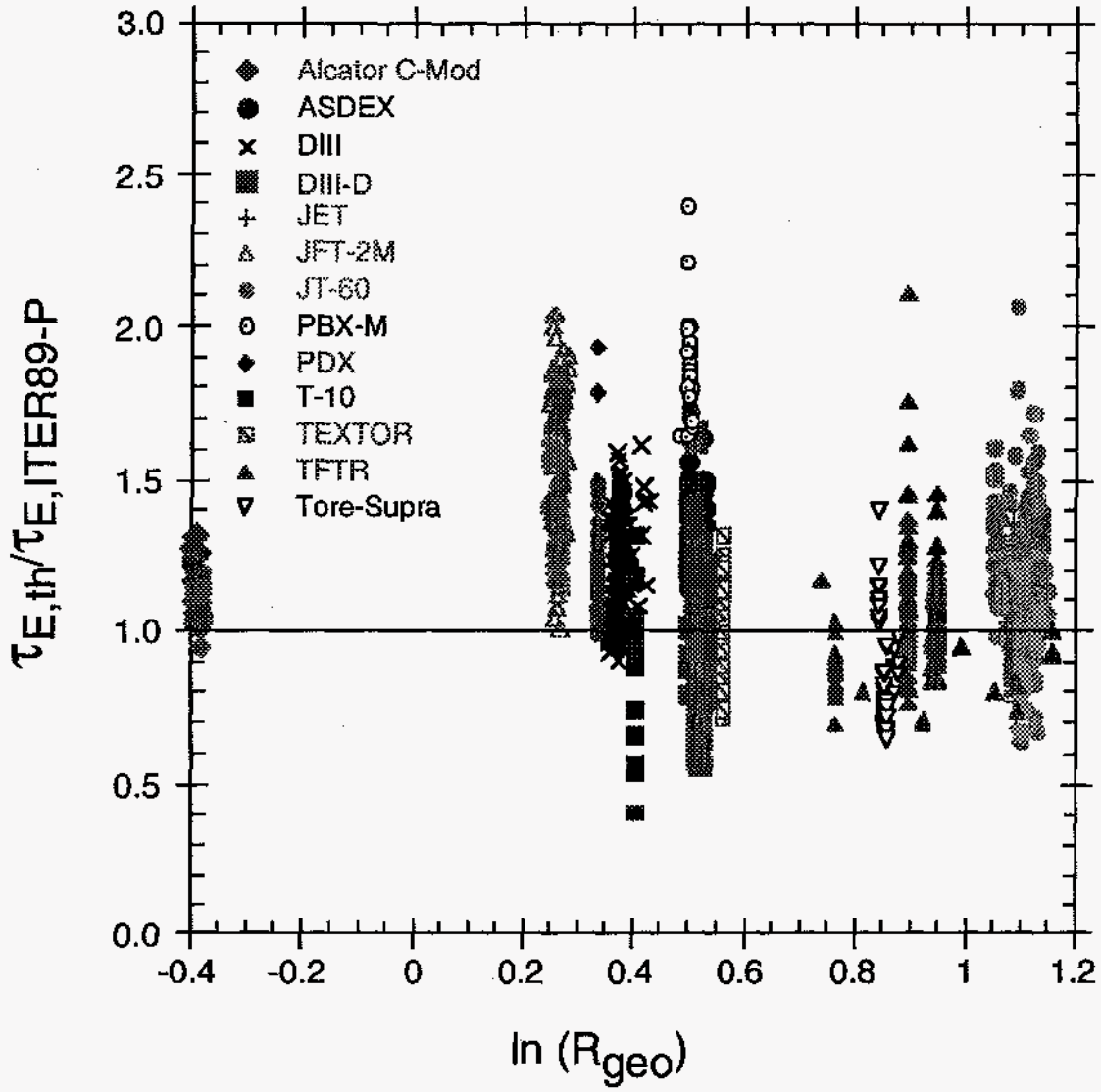

Fig. 4 Ratio of the total energy confinement time relative to that given by the ITER89-P scaling for each device.

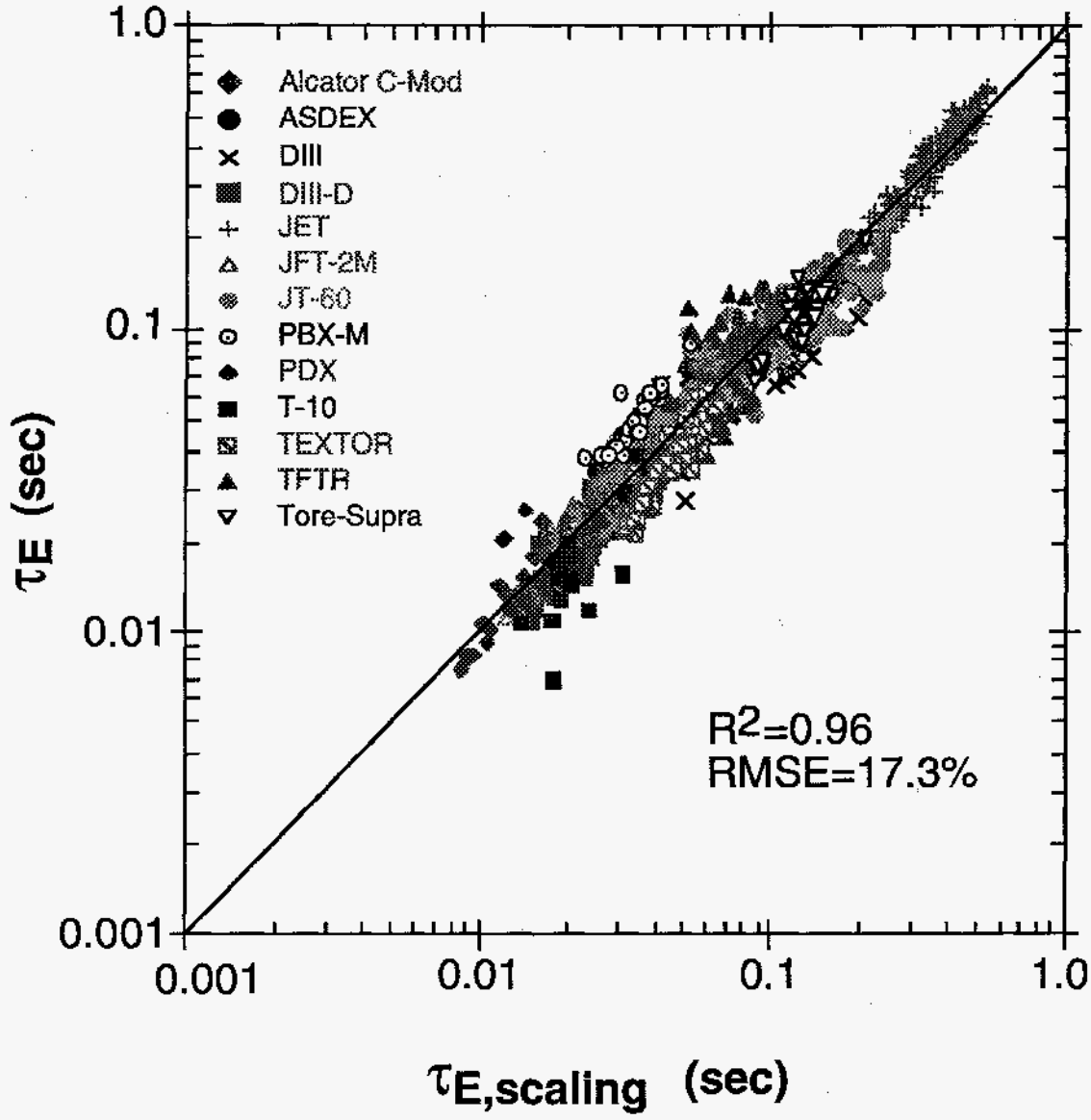

Fig. 5 Total experimental energy confinement time plotted as a function of the scaling value. The line corresponds to $\tau_E=\tau_{E,scaling}$.

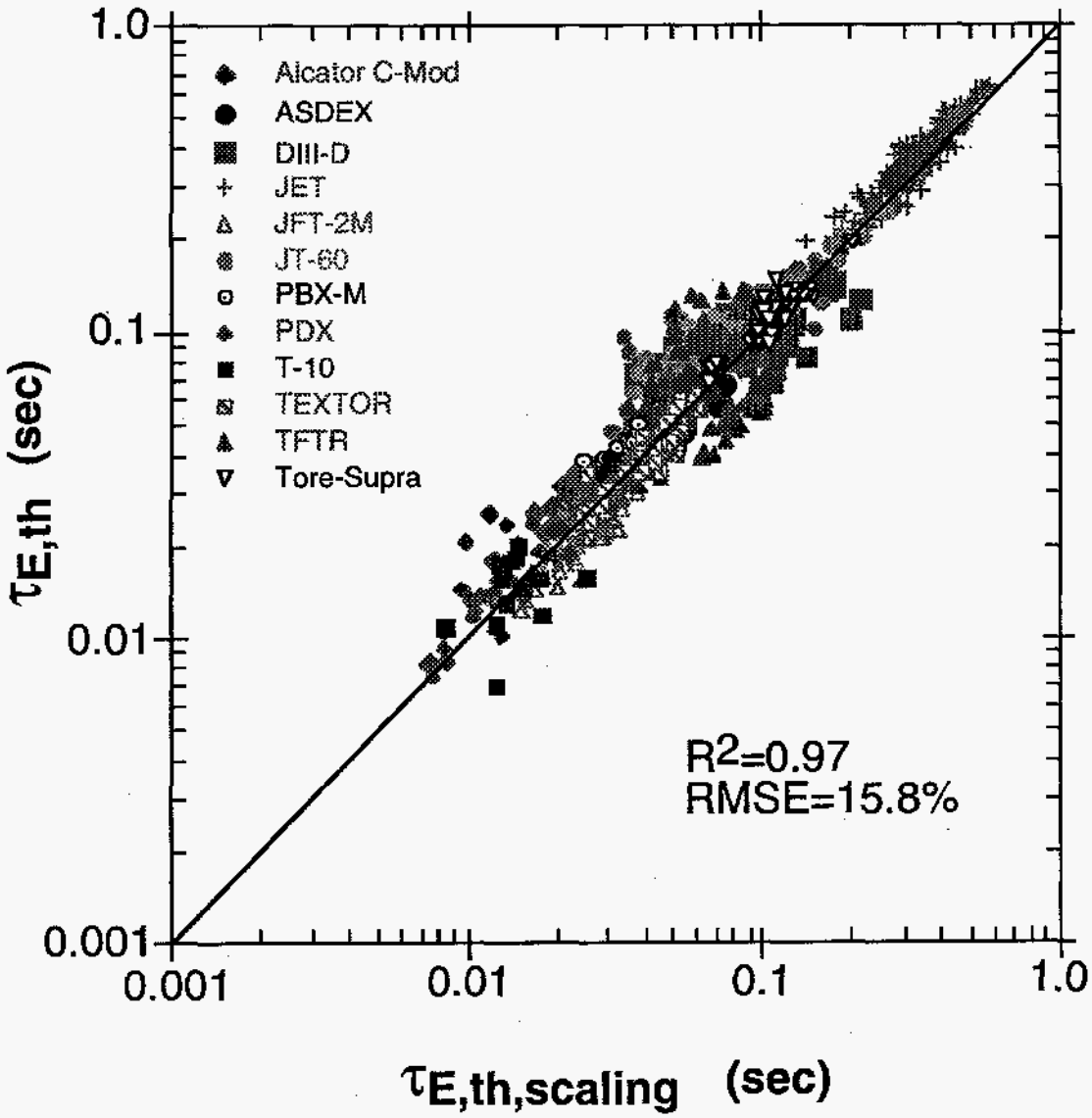

Fig. 6 Thermal experimental energy confinement time plotted as a function of the scaling value. The line indicates $\tau_{E,th}=\tau_{E,th,scaling}$.

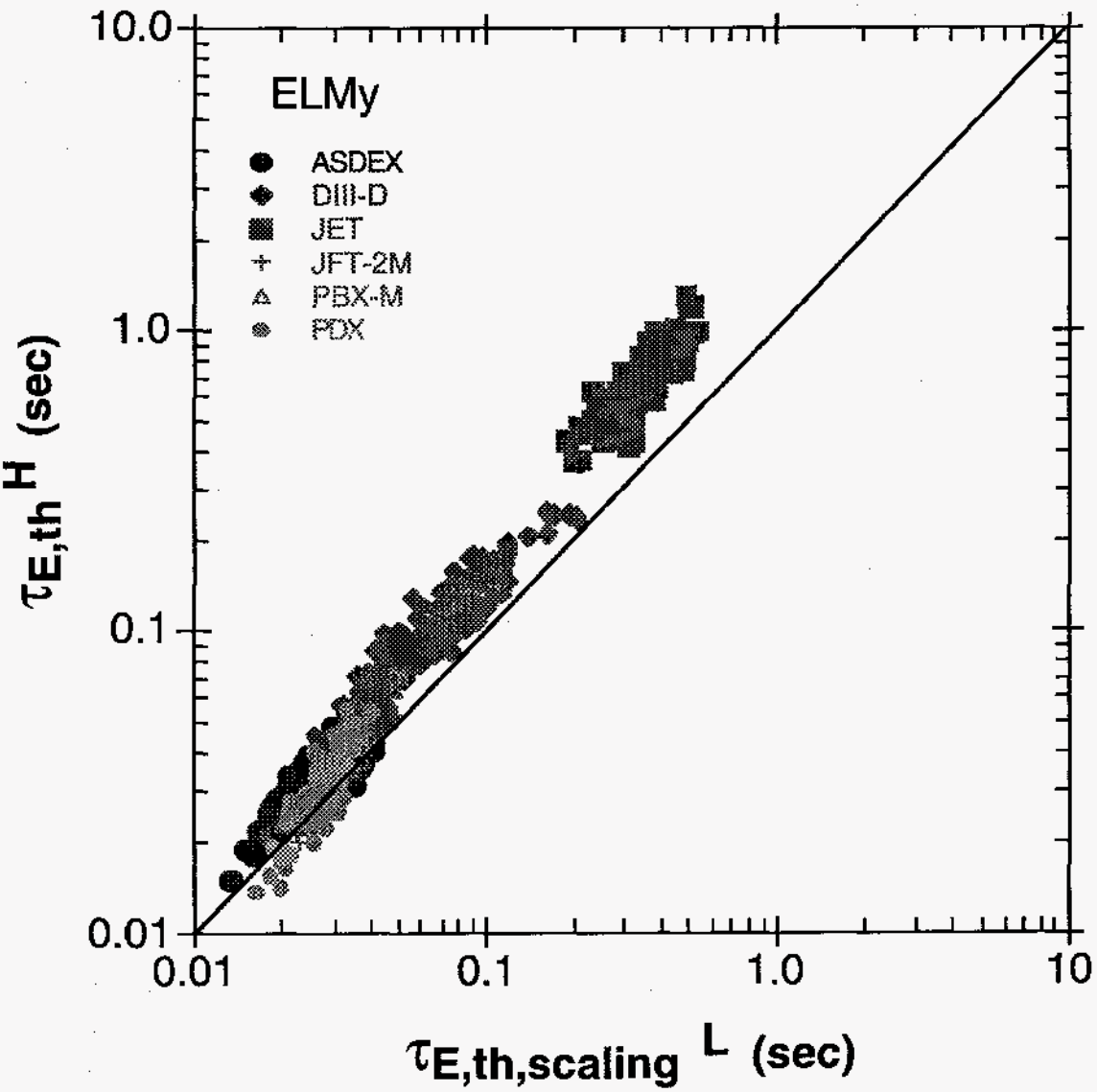

Fig. 7 Thermal experimental energy confinement time of the standard subset of ELMy discharges in the H-mode database plotted as a function of the L-mode thermal confinement time scaling value. The line indicates $\tau_{E,th}{}^{H}=\tau_{E,th,scaling}{}^{L}$.

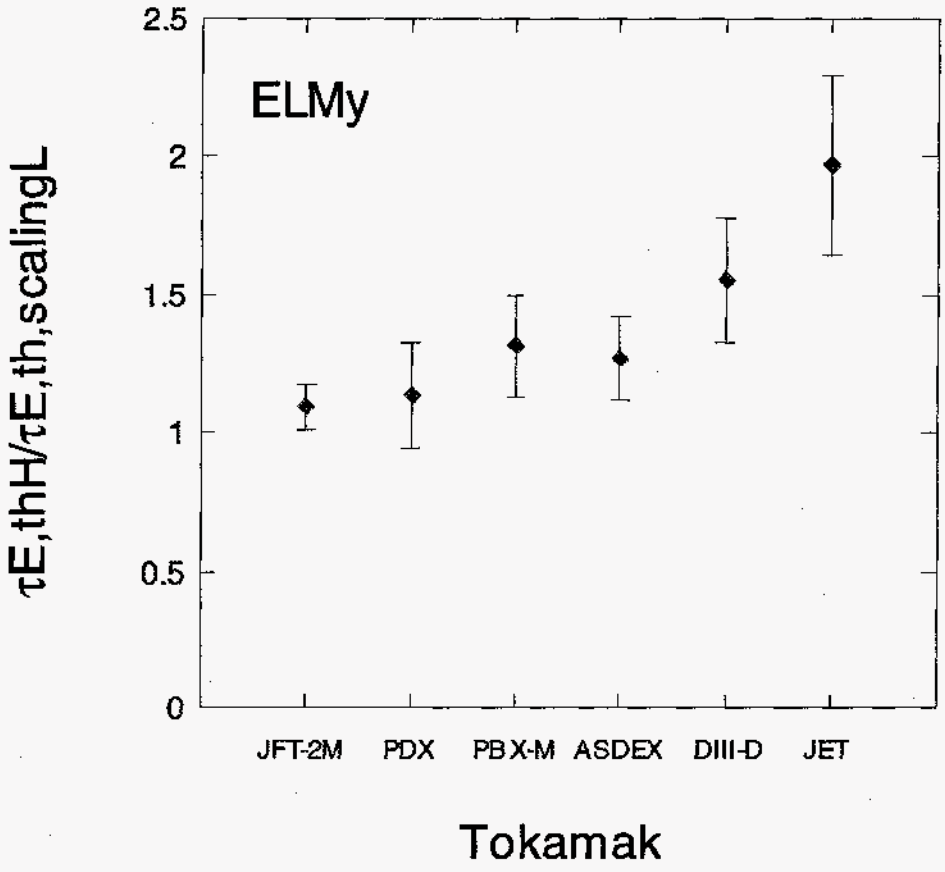

Fig. 8 Ratios of the ELMy H-mode thermal confinement time to that of the L-mode scaling. The error bars correspond to the standard deviations of the ratios.

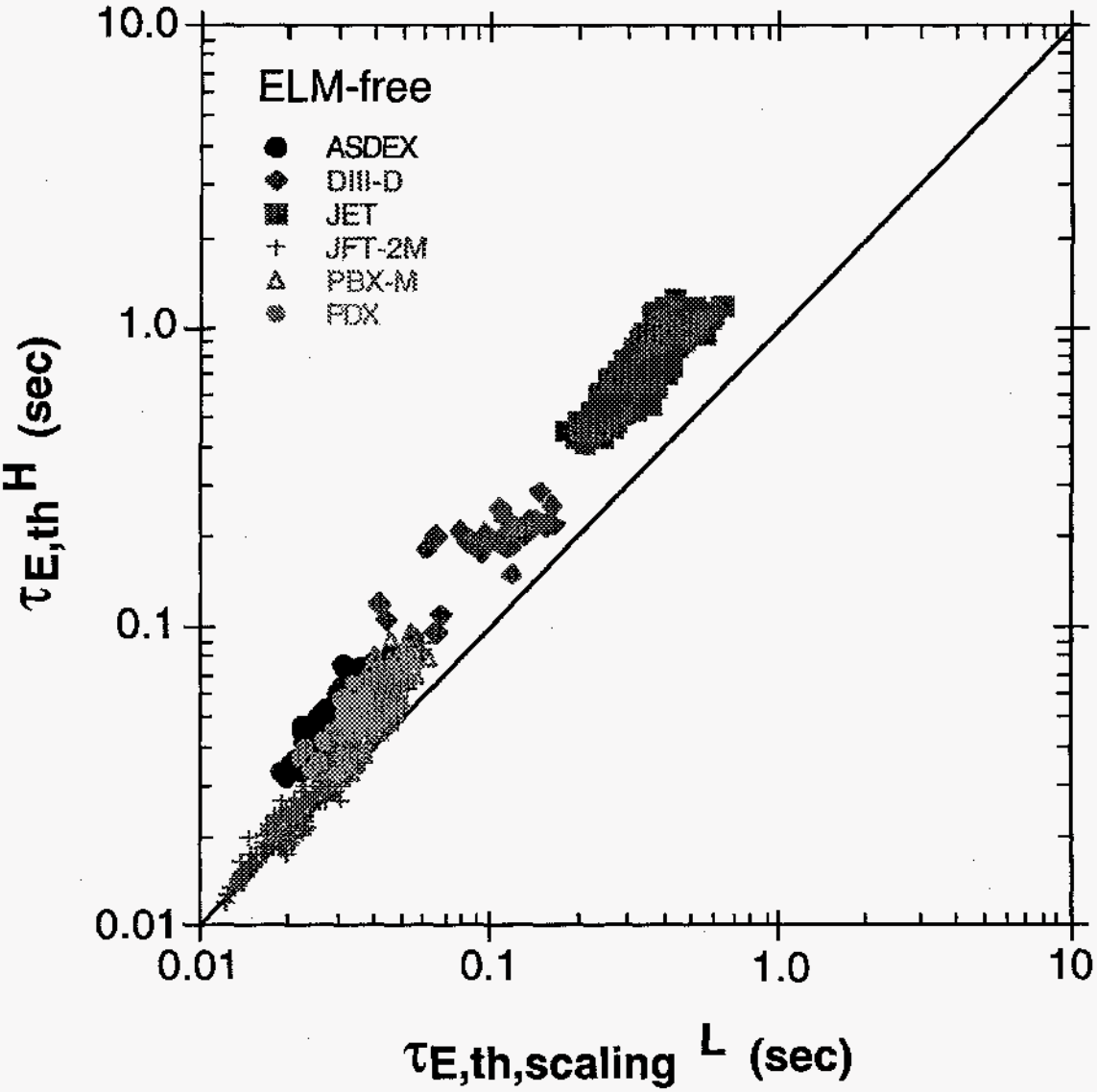

Fig. 9 Thermal experimental energy confinement time of the standard subset of ELM-free discharges in the H-mode database plotted as a function of the L-mode thermal confinement time scaling value. The line indicates $\tau_{E,th}^{H}=\tau_{E,th,scaling}^{L}$.

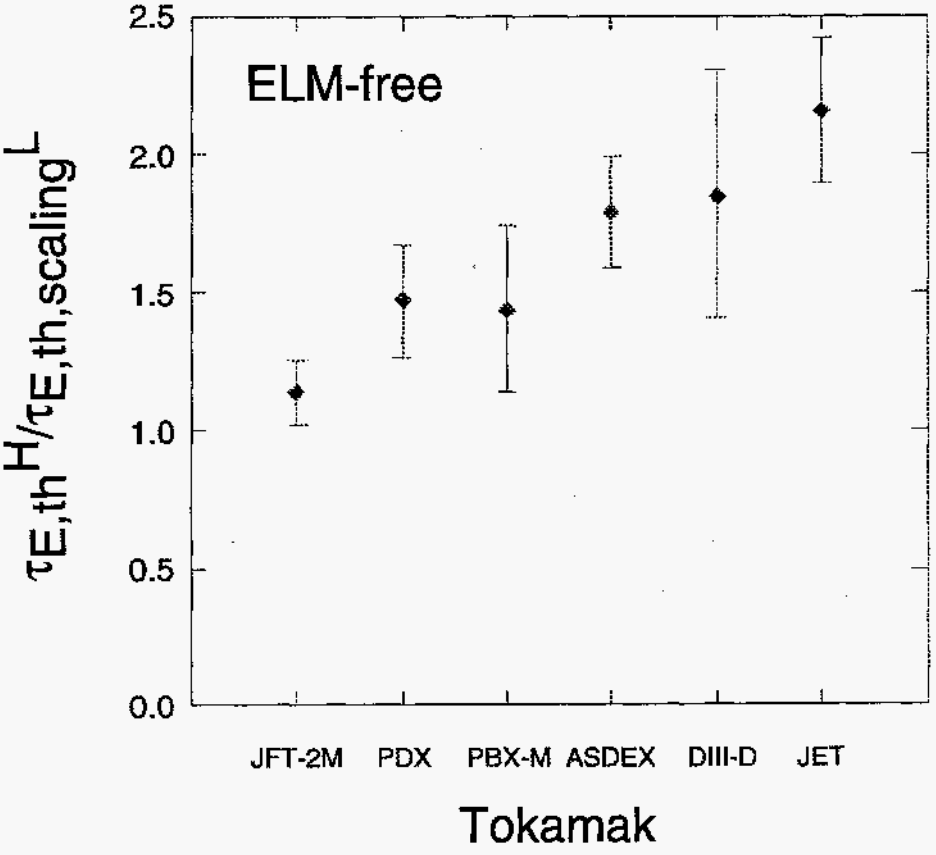

Fig. 10 Ratios of the ELM-free H-mode thermal confinement time to that of the L-mode scaling. The error bars correspond to the standard deviations of the ratios.